

# Ion transport in a model gramicidin channel

## Structure and thermodynamics

Benoît Roux and Martin Karplus

Department of Chemistry, Harvard University, Cambridge, Massachusetts 02138 USA

Marine Biological Laboratory  
LIBRARY

MAY 8 1991

Woods Hole, Mass.

**ABSTRACT** The potential of mean force for  $\text{Na}^+$  and  $\text{K}^+$  ions as a function of position in the interior of a periodic poly(L, D)-alanine model for the gramicidin  $\beta$ -helix is calculated with a detailed atomic model and realistic interactions. The calculated free energy barriers are 4.5 kcal/mol for  $\text{Na}^+$  and 1.0 kcal/mol for  $\text{K}^+$ . A decomposition of the free energy demonstrates that the water molecules make a significant contribution to the free energy of activation. There is an increase in entropy at the transition state associated with greater fluctuations. Analysis reveals that the free energy profile of ions in the periodic channel is controlled not by the large interaction energy involving the ion but rather by the weaker water–water, water–peptide and peptide–peptide hydrogen bond interactions.

The interior of the channel retains much of the solvation properties of a liquid in its interactions with the cations. Of particular importance is the flexibility of the helix, which permits it to respond to the presence of an ion in a fluidlike manner. The distortion of the helix is local (limited to a few carbonyls) because the structure is too flexible to transmit a perturbation to large distances. The plasticity of the structure (i.e., the property to deform without generating a large energy stress) appears to be an essential factor in the transport of ions, suggesting that a rigid helix model would be inappropriate.

## INTRODUCTION

The relation of structure to function of transmembrane ion channels is of central concern for physiologists. Unfortunately, the relative intractability of biological membrane proteins poses severe problems for the characterization of ion permeation in molecular terms. Due to the lack of structural information about biological channels, progress in understanding the mechanisms of ion permeation has been made by studying the properties of simple pore forming molecules such as the gramicidin A (1). Even though the gramicidin A molecule is thought not to act as a channel in nature (2), its great simplicity and its functional behavior, similar to that of more complex biological channels, have made it an ideal model system to study ion permeation through membranes. It is presently the best characterized transmembrane channel molecule (3). In particular, the transport of monovalent cations in the gramicidin A channel has been the object of numerous experimental studies (4–7).

The gramicidin A channel acts, as do most biological channels, by providing an efficient and energetically favorable pathway for the passage of ions through lipid membranes. An understanding of the rate of ion passage through the channel and the origin of selectivity requires a knowledge of both the dynamic and thermodynamic factors involved. The free energy profile along the channel, a concept essential to modern discussions of rate processes, in general (8, 9), and of ion transport in particular (1, 10–13), is thought to be the main factor

responsible for the selectivity. Purely dynamical factors are believed to be less important. For example, the free energy profile of monovalent cations in the gramicidin A channel is thought to be mainly responsible for the selectivity sequence observed experimentally ( $\text{Li}^+ < \text{Na}^+ < \text{K}^+ < \text{Rb}^+ < \text{Cs}^+$ ) (6). The free energy profile, which corresponds to the potential of mean force, is the reversible work  $\mathcal{W}(x)$  needed to move an ion along the axis of the channel. Given an estimate of the free energy profile  $\mathcal{W}(x)$ , a variety of dynamical models, such as classical transition state theory (14–16), Nernst-Planck continuum diffusion theory (17), Brownian dynamics stochastic simulations (13) and activated dynamics methodologies (18) can be used to provide a complete description of the properties of a channel, including the ion permeabilities, the rate of transport and the response to an applied electrical potential. Analysis of data from single channel conductance experiments based on classical transition state theory has indicated that the overall activation free energy barriers are on the order of 5–10 kcal/mol (1, 4, 6, 19). However, the microscopic nature and detailed origin of the free energy profiles of the cations in the gramicidin A channel are not known and have led to considerable speculation (6).

Advances in computer simulations of complex biological systems (20) make it possible to study the properties of the gramicidin A channel at the atomic level. There have been several attempts at calculating the free energy profile with detailed models. Jordan studied the poten-

tial of mean force of  $\text{Cs}^+$  ion along the axis of a polyglycine analogue of the gramicidin channel using the umbrella sampling method (21). The results obtained are qualitatively similar to calculations on  $\text{Cs}^+$  ion by Mackay, D. H., P. M. Edelsten, and K. R. Wilson (unpublished results; reported in reference 12). The main activation barrier, ~16 kcal/mol in the calculation of Jordan and 40 kcal/mol in the calculation of Mackay et al., was found at the entrance of the channel where bulklike solvation is transformed into single-file solvation. No large barriers were observed inside the channel. Ålquist and Warshel (22) have calculated the free energy profile of  $\text{Na}^+$  ion along the gramicidin channel and obtained results that appears to be in better agreement with the experimental estimates. However, a mixed method was used, combining some detailed aspect of the interactions of the ion with the nearest neighbors and a continuum electrostatic representation of the distant neighbors (membrane and waters). The interaction energy profile of  $\text{Na}^+$ , which is of relevance in the determination of the free energy profile, was calculated adiabatically with energy minimization by Pullman (23), and with Monte Carlo simulations by Kim and Clementi (24); both calculations yielding an energy barrier of ~20 kcal/mol at the entrance.

Difficulties in calculating the free energy profile can arise from various aspects of the models, including a possible imbalance in the parametrization of ion-channel, ion-water and water-channel interactions. For detailed simulations to be meaningful, accurate empirical potential functions have to be used. This is particularly true in a highly confined system, such as the gramicidin A channel, where there is a severe competition among the polar interactions. It is essential that the simulation be based on a model which correctly treats the relative effects of the strong cation-carbonyl and cation-water interactions, and the weaker but more complex water–water, water–peptide and peptide–peptide hydrogen bonding interactions.

The goals of this and subsequent papers are to explore the ion-gramicidin system by means of simulations and rate theory analysis with detailed atomic model involving realistic interactions. The empirical energy function used in the present study was derived from high level *ab initio* quantum-mechanical calculations and solvation simulations (Reiber III, W., and M. Karplus, unpublished results; Roux, B., and M. Karplus, unpublished results). This paper concentrates on the translocation mechanism in the interior of the channel where the ion is in the presence of only a few water molecules in single file. To examine this aspect of the problem a molecular dynamics simulation was done on an infinite periodic poly(L, D)-alanine  $\beta$ -helix model for the channel. Such a

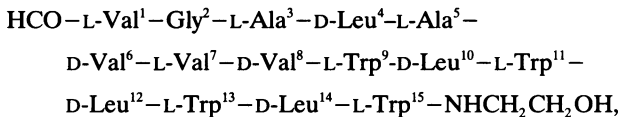
periodic helix is appropriate for treating the motion within a monomer, because ends effects and sidechains are expected to play a secondary role for the free energy barriers of the interior of the pore (25). The dynamics of the ion in the channel (18) and the behavior at the channel entrance and at the monomer boundary will be addressed in future work. Further, although solute-solute potential of mean force are now calculated almost routinely in bulk solution with Monte Carlo (26) or molecular dynamics (27, 28) simulations, the high confinement of the cation and water inside the gramicidin channel is a likely source of difficulty. Problems of insufficient equilibration may introduce nonequilibrium hysteresis in the free energy profile due to incomplete relaxation of the system (29). The virtue of the periodic system is that it makes possible the detection of any hysteresis and insufficient equilibration in the calculation of the potential of mean force, i.e., because the free energy profile is a periodic function of the position of the ion along the axis, any deviations from periodicity found in the simulations indicate lack of convergence of the results. Moreover, the symmetry of the system is such that the free energy profile is independent of the handedness of the periodic helix. This is an advantage because there remains some uncertainty concerning the structure of the conducting gramicidin A channel in lipid bilayers. Proton–proton NOE distances determined by two-dimensional NMR experiments have demonstrated that the structure of gramicidin A is a right-handed  $\beta$ -helix head-to-head dimer when incorporated in SDS micelles (30), in contrast to the left-handed  $\beta$ -helix that was originally proposed by D. W. Urry (31) and supported by  $^{13}\text{C}$   $\text{Na}^+$  induced chemical shifts measurements in lecithin vesicles (32). Recent solid state  $^{15}\text{N}$  and  $^{13}\text{C}$  NMR for gramicidin in oriented dimyristoylphosphatidylcholine (DMPC) membranes results have been used to support both the left-handed (33, 34) and right-handed (35, 36) structures. In view of the extreme sensitivity of gramicidin to the environment (37), it may well be that both the left- and right-handed helices, which are plausible on energetic and structural grounds, are found in membranes. The present study of the properties of the periodic  $\beta$ -helix represents a first step toward the understanding of the complete channel, whether it is left- or right-handed.

The periodic  $\beta$ -helix model system and the potential function are introduced and described in detail in the next section. The free energy profile of  $\text{Na}^+$  and  $\text{K}^+$  ions in the channel and the effect of the channel on the water are calculated and analyzed structurally and thermodynamically in the following sections. The discussion outlines some of the important conclusions from the present study and its relation to future work.

## METHODOLOGY

### Atomic model and potential function

The interior of the gramicidin A channel, which has the composition



is represented as a periodic poly (L, D)-alanine  $\beta$ -helix; the sidechains of gramicidin were neglected to simplify the system and introduce periodicity. The periodic helix is taken to be representative of the interior of the channel away from the intermonomer contact (at the formyl group end) and from the channel mouth (at the ethanolamine group end); i.e., from L-Ala<sup>3</sup> to D-Leu<sup>10</sup> in the gramicidin A dimer. Alanines residues were chosen because the gramicidin monomer has only one glycine residue and all the other residues yield  $\phi$ ,  $\psi$  energy map that are similar to alanine. The transformation from left- to right-handed helix is obtained by making the substitution D-Ala  $\leftrightarrow$  L-Ala, and by changing the sign of all the  $\phi$  and  $\psi$  dihedrals, i.e., it is a mirror transformation of the coordinates. Because neither an ion nor a water molecule has a chiral center, the free energy profile in the periodic  $\beta$ -helix is independent of handedness.

A periodic  $\beta$ -helix structure was initially constructed using the  $\phi$  and  $\psi$  angles from Urry and Ventakachalam (38) (see Table 1) and refined in the absence of any ion and solvent molecules. The helical parameters, the rise and the rotation angle per helical unit (L-Ala, D-Ala), were optimized by energy minimization with the ABNR algorithm (39). It was found that the optimum rise per unit,  $\Delta L$ , is 1.55 Å and the optimum rotation per unit,  $\theta$ , is 114.4 degrees, yielding 6.29 residue per turn; this value is essentially the same as that of the Urry helix model (6.3) (33). The residue dihedral angles are listed in Table 1. The fundamental unit, treated with periodic boundary conditions to avoid end effects (images of the system are repeated along the helix axis), includes 34 alanine residues, a cation, and eight water molecules. The total number of particles is 229. The system has a length of 26.35 Å, larger than twice the nonbonded cutoff (12 Å, see below) to reduce any spurious effects due to the periodicity. The number of water molecules included was based on their average diameter (~2.8 Å), the diameter of Na<sup>+</sup> ion (1.8 Å), and the total length of the system. The initial Na<sup>+</sup> system was constructed by putting the ion at the center of the channel (near L-Ala<sup>15</sup>) and placing the eight water molecules in single file, four on each side of the ion in the optimized helix. The helix is oriented along the x-axis and the 34 alanine residues are numbered from the NH<sub>2</sub>-terminus to the COOH-terminus, the odd numbered L-alanine

carbonyls pointing toward the NH<sub>2</sub>-terminus (+x) and the even numbered D-alanine carbonyls pointing toward the COOH-terminus (-x). The initial coordinates of the full periodic system were optimized by energy minimization using the ABNR algorithm (39). The system was then equilibrated at 300° K for 10 ps with the ion constrained at x = 0 but free to move in the y and z directions. No constraints were applied on the helix to maintain the  $\beta$ -helical conformation, in contrast to other studies (40). It should be stressed, however, that the periodic boundary conditions applied on the system do increase the stability of the  $\beta$ -helical structure by removing any end effects and imposing a fixed length to the 34 residues polypeptide. The full system in the presence of Na<sup>+</sup> ion is shown in Fig. 1. A water-filled channel, in which the Na<sup>+</sup> ion is replaced by a ninth water molecule, was also constructed and a 250 ps trajectory was generated to provide a reference system without ions.

In the atomic model all heavy atoms and all polar hydrogens (those able to form hydrogen bonds) are included. The aliphatic hydrogens are treated as part of the carbon to which they are attached in an extended atom model. The water-water (TIP3P) (41), peptide-peptide and water-peptide (CHARMM) (39) potential functions have been described elsewhere. Special care was given to the parametrization of the interaction of the ion with the channel and water. *Ab initio* calculations were made of the interactions of Na<sup>+</sup> with the acetamide molecule, taken as a model of the peptide carbonyl group. Both the radical and angular dependence of the interaction of the Na<sup>+</sup> with the carbonyl group were explored. The radial dependence along the C = O bond direction is shown in Fig. 2. It was found that a good description of the Na<sup>+</sup> ion-channel interaction is given by

$$E_{i-c} = E_{vdw} + E_{elec} + E_{pol}, \quad (1)$$

where  $E_{vdw}$  is the van der Waals interaction,  $E_{elec}$  is a standard electrostatics interaction between the ion and the partial charge of the peptide atoms, and  $E_{pol}$  is an attractive charge-induced dipole interaction. Except for the polarization term  $E_{pol}$ , Eq. 1 is the standard nonbonded empirical potential energy function used in computer simulations of macromolecular systems (20). The ion-carbonyl oxygen van der Waals interaction  $E_{vdw}$  is represented by a  $\sim 1/r^8$  core repulsion, significantly softer than the more standard  $\sim 1/r^{12}$  repulsion of the Lennard-Jones 6–12 potential. In general, softer repulsive functions are thought to give a better representation of the core interaction caused by the Pauli exclusion principle for the temperatures used in biopolymer simulations (42). In the case of the strong ion-carbonyl oxygen electrostatic interaction the use of a softer core was found to be necessary to reproduce the *ab initio* calculations. The other van der Waals Lennard-Jones 6–12 interactions parameters (39) and the electrostatic partial charges used in  $E_{elec}$  have been taken from previous work. The polarization interaction  $E_{pol}$  arises from the interaction between the charge of the ion and the point dipole induced on the peptide atoms (43–45). Such a term is required to obtain the steeper-than-Coulombic distance dependence of the ion-peptide interaction in the range of 2–5 Å (see Fig. 2). It is written as a sum over terms depending only on  $r_i$ , the distance between the ion and the  $i$ th helix atom,

$$E_{pol} = \sum_i -\frac{1}{2} \frac{q^2 \alpha_i}{r_i^4}, \quad (2)$$

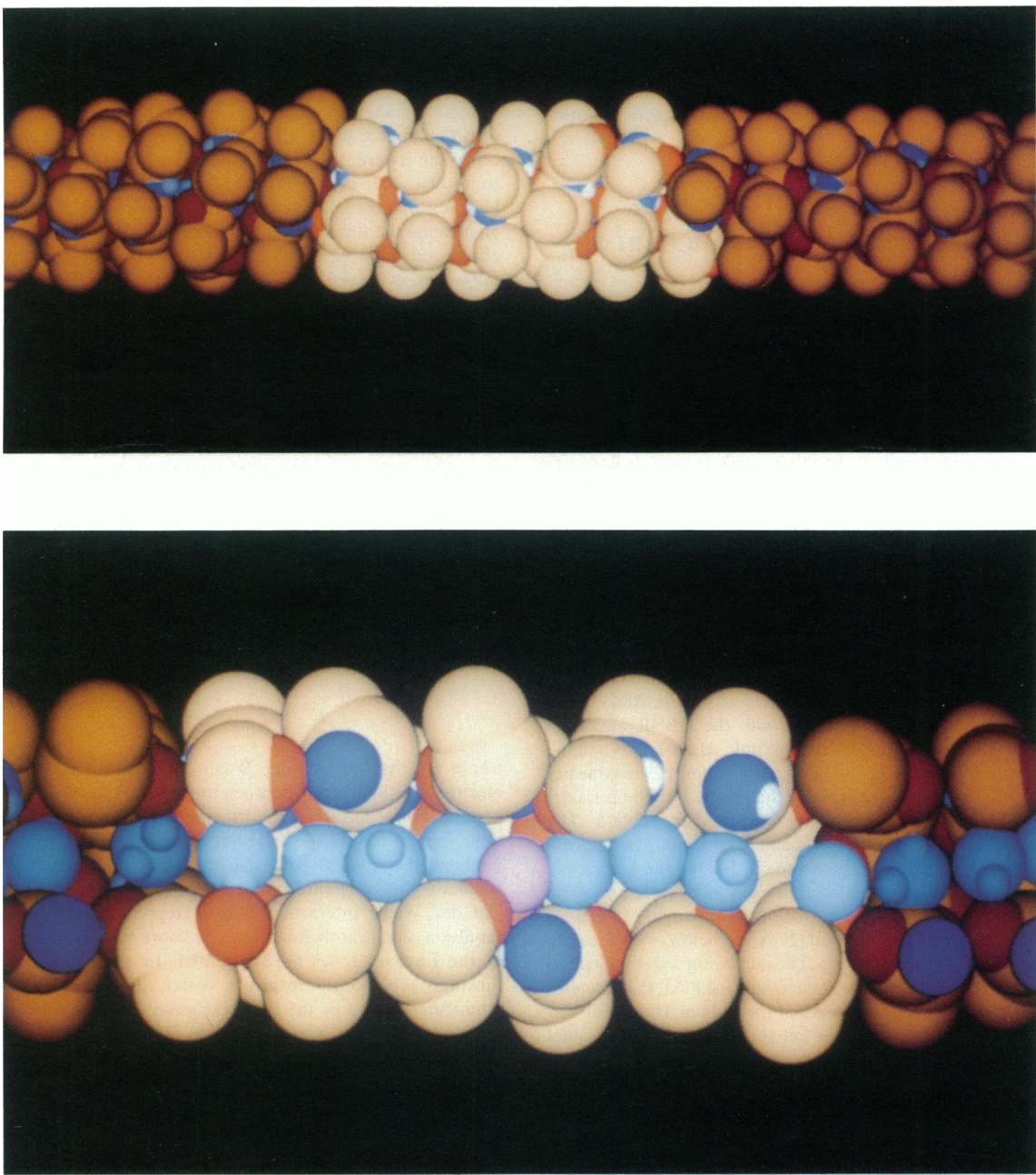
where  $q$  is the charge of the ion and  $\alpha_i$  is the atomic polarizability of helix atom  $i$ . Only the dominant first-order polarization induced by the ion on the peptide was included; i.e., the partial charges of the peptide and the water as well as other induced dipoles do not influence a

TABLE 1 Left-handed  $\beta$ -helix structures\*

Dihedral angles	Energy minimization	Molecular dynamics <sup>†</sup>
$\phi$ L-ala	-139	-133 (15)
$\psi$ L-ala	123	117 (17)
$\phi$ D-ala	114	-115 (18)
$\psi$ D-ala	-125	-128 (13)

\*The right-handed helix is obtained by changing the sign of the dihedrals and the chirality of the amino acids.

<sup>†</sup>From the 250 ps molecular dynamics simulation with 9 water molecules.



**FIGURE 1** Space filling representation of the  $\text{Na}^+$  ion in the periodic  $\beta$ -helix with the eight water molecules seen from the outside (*top*) and seen through a cut across the channel (*bottom*). The helix is represented as left handed, although the statistical results are independent of helix handedness. The images of the periodic boundary conditions are shown in dim light. The picture was generated with the program QUANTA (Polygen Corporation, Waltham, MA).

particular induced dipole. The polarizabilities were chosen to reproduce the *ab initio* calculations and the values are similar to other atomic polarizabilities (39). All the ion interaction parameters used in the calculation are reported in Tables 2–4. The ion-oxygen carbonyl, using the acetamide molecule as a peptide model, and ion-water oxygen optimized geometries and interaction energies are also given in Tables 3 and 4. Due to the significant contribution of electrostatic

energy to the dynamics of an ion, a relatively large group-based cutoff of 12 Å was used for the nonbonded interactions.

### Potential of mean force

The potential of mean force of the ion along the channel axis is calculated using the free energy simulation technique (27, 46). The

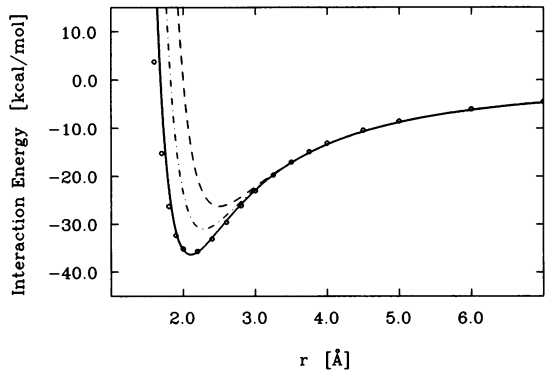


FIGURE 2 Dependence of the interaction energy on the ion-oxygen distance along the C=O bond of the acetamide molecule. The circles represent the results of *ab initio* calculations for  $\text{Na}^+$  ion (26) using the HF/6-31G\* basis set, the solid line is the empirical energy including the polarization as described in the text. The dashed line represents the empirical interaction energy for the first  $\text{K}^+$  model. The dot-dashed line represents the case of an intermediate fictitious ion larger than  $\text{Na}^+$  and smaller than  $\text{K}^+$  as used in Fig. 18. See also the ion-carbonyl optimized geometry data in Table 3.

free energy of the system,  $\mathcal{W}(x)$ , as a function of the coordinate  $x$  of the ion is proportional to the configuration integral (17),

$$e^{-\mathcal{W}(x)/k_B T} \alpha \int dR e^{-U(R, x)/k_B T}, \quad (3)$$

where  $U(R, x)$  is the total potential energy of the system for the  $x$  coordinate of the ion constrained at the position  $x$ ,  $R$  represents all the remaining coordinates of the system (the  $x, y, z$  coordinates of all the channel and water atoms plus the  $y$  and  $z$  coordinates of the ion), and  $dR$  is the volume element in configuration space. From Eq. 3, the potential of mean force at a position  $\mathcal{W}(x + \Delta x)$  can be expressed in terms of  $\mathcal{W}(x)$

$$\Delta\mathcal{W}(x \rightarrow x + \Delta x) = \mathcal{W}(x + \Delta x) - \mathcal{W}(x) = -k_B T \ln \langle e^{-\Delta U/k_B T} \rangle_{(x)}, \quad (4)$$

where the bracket with subscript  $x$  represents a canonical average with the reaction coordinate held fixed at  $x$ , that is,

$$\langle e^{-\Delta U/k_B T} \rangle_{(x)} = \frac{\int dR e^{-\Delta U/k_B T} e^{-U(R, x)/k_B T}}{\int dR e^{-U(R, x)/k_B T}}, \quad (5)$$

TABLE 2 Interaction parameters

Atom	$\sigma$	$\epsilon$	$q$	$\alpha$
	$\text{\AA}$	$\text{kcal/mol}$	$\epsilon$	$\text{kcal/mol} \text{\AA}^4/e$
$\text{Na}^+$	2.7297	0.1000	1.00	—
$\text{K}^+$	3.3605	0.3600	1.00	—
C	3.2072	0.0498	0.55	0.3
O	2.8509	0.1591	-0.55	1.5
N	2.8509	0.2384	-0.35	1.5
H	1.4254	0.8000	0.25	0.0
C <sup>a</sup>	3.8576	0.1142	0.10	0.5

TABLE 3 Ion-carbonyl parameters<sup>\*\*</sup>

Ion	$A^{(8)}$	$B^{(6)}$	$R_{\min}$	$E_{\min}$
	$\text{kcal/mol} \text{\AA}^8$	$\text{kcal/mol} \text{\AA}^6$	$\text{\AA}$	$\text{kcal/mol}$
Na	6,200	290	2.10	36.3
$\text{K}_I^+$	17,000	800	2.49	26.6
$\text{K}_{II}^+$	30,000	3,600	2.50	29.2

\*The Lennard-Jones 8–6 function is  $A^{(8)}/r^8 - B^{(6)}/r^6$ .

<sup>\*\*</sup>The optimized distances  $R_{\min}$  and energies  $E_{\min}$  were calculated with the acetamide molecule.

and  $\Delta U$  is the change in potential energy obtained by displacing the ion from  $x$  to  $x + \Delta x$ , i.e.,  $\Delta U$  is equal to  $U(R, x + \Delta x) - U(R, x)$ . Eq 5 is evaluated by a computer simulation for an equilibrated system with the ion fixed at  $x$ . Although Eq. 4 is formally valid for any  $\Delta x$ , convergence in achievable computer times limits the calculation to the free energy differences in the neighborhood of  $x$ . The full profile is constructed by joining the free energy differences obtained with Eq. 4 at the midpoints between neighboring simulations, that is,

$$\begin{aligned} \mathcal{W}(x_{n+1}) &= \mathcal{W}(x_n) + \Delta\mathcal{W}(x_n \rightarrow x_n + \Delta x) \\ &\quad - \Delta\mathcal{W}(x_{n+1} \rightarrow x_{n+1} - \Delta x) \\ &= \sum_{i=1}^n [\Delta\mathcal{W}(x_i \rightarrow x_i + \Delta x) \\ &\quad - \Delta\mathcal{W}(x_{i+1} \rightarrow x_{i+1} - \Delta x)], \end{aligned} \quad (6)$$

where  $\Delta x$  is the middistance between two neighboring simulations.

$$\Delta x = \frac{|x_{n+1} - x_n|}{2}. \quad (7)$$

The free energy profile can also be calculated by integrating the reversible work done by the mean force  $\langle F(x) \rangle$  acting on the ion in the  $x$  direction; that is,

$$\mathcal{W}(x) = \mathcal{W}(x_0) - \int_{x_0}^x \langle F(x') \rangle dx', \quad (8)$$

where the value of  $\mathcal{W}(x_0)$  is arbitrarily chosen, so that only relative values of  $\mathcal{W}(x)$  are obtained. Eq. 8 is the reason why the free energy profile is called a potential of mean force (47). One advantage of this formulation is that the mean force can be decomposed linearly into a sum of contributions, e.g.,

$$\langle F(x) \rangle = \sum_{\alpha} \langle F_{\alpha}(x) \rangle, \quad (9)$$

and the linearity, preserved by the integral of the mean force along the reaction coordinate allows one to determine the contribution  $\mathcal{W}_{\alpha}(x)$  of

TABLE 4 Ion-water parameters<sup>†</sup>

Ion	$A^{(12)}$	$B^{(6)}$	$R_{\min}$	$E_{\min}$
	$\text{kcal/mol} \text{\AA}^{12}$	$\text{kcal/mol} \text{\AA}^6$	$\text{\AA}$	$\text{kcal/mol}$
$\text{Na}^+$	83,000	440	2.20	27.4
$\text{K}^+$	330,000	300	2.62	19.6

\*The Lennard-Jones 6–12 function is  $A^{(12)}/r^{12} - B^{(6)}/r^6$ .

<sup>†</sup>The optimized distances  $R_{\min}$  and energies  $E_{\min}$  were calculated with the TIP3P water molecule<sup>(41)</sup>.

any interaction term to the potential of mean force

$$\mathcal{W}(x) = \sum_a \mathcal{W}_a(x), \quad (10)$$

with

$$\mathcal{W}_a(x) = \mathcal{W}_a(x_0) - \int_{x_0}^x \langle F_a(x') \rangle dx'. \quad (11)$$

The mean force contribution of the water and the channel to  $\mathcal{W}(x)$  were computed from Eqs. 9–11. The arbitrary zero of the potential of mean force,  $x_0$ , was chosen at the position of the free energy minimum of  $\mathcal{W}(x)$ . The total potential of mean force can be computed equivalently with the free energy simulation technique, via Eq. 4 via Eq. 8. However, the mean force decomposition can only be obtained with the latter method using Eqs. 9–11. The formulation used here is equivalent to the thermodynamic integration (47, 48) with the coupling parameter corresponding to the  $x$  coordinate.

Using the simulation technique, it is also possible to obtain the average of any quantity of interest  $Q(x)$  at a perturbed position  $x + \Delta x$ . The canonical average of an observable  $Q(x + \Delta x)$  in the presence of an ion constrained at  $x + \Delta x$  is

$$\langle Q(x + \Delta x) \rangle_{(x+\Delta x)} = \frac{\int dR Q(x + \Delta x) e^{-U(R,x+\Delta x)/k_B T}}{\int dR e^{-U(R,x+\Delta x)/k_B T}}. \quad (12)$$

The integrals in Eq. 12 can be rewritten in terms of a canonical average obtained with the ion constrained at  $x$ . That is,

$$\langle Q(x + \Delta x) \rangle_{(x+\Delta x)} = \frac{\langle Q(x + \Delta x) e^{-\Delta U/k_B T} \rangle_{(x)}}{\langle e^{-\Delta U/k_B T} \rangle_{(x)}}, \quad (13)$$

where  $\Delta U$  and the denominator have the same meaning as in Eq. 5, and the numerator represents

$$\langle Q(x + \Delta x) e^{-\Delta U/k_B T} \rangle_{(x)} = \frac{\int dR Q(x + \Delta x) e^{-\Delta U/k_B T} e^{-U(R,x)/k_B T}}{\int dR e^{-U(R,x)/k_B T}}. \quad (14)$$

This expression is useful to obtain the average of a quantity in the neighborhood of a simulation. For example, Eq. 13 is used to calculate the forces acting on the ion at perturbed positions to obtain a more accurate result in Eq. 11. If one is interested in the relative value of the canonical average of  $Q$  as a function of  $x$ , Eq. 13 is not useful in general because the statistical convergence is too slow. Better convergence is obtained by considering the average increment ( $\Delta Q$ ) in going from  $x$  to  $x + \Delta x$ ,

$$\begin{aligned} \langle \Delta Q(x \rightarrow x + \Delta x) \rangle &= \langle Q(x + \Delta x) \rangle_{(x+\Delta x)} - \langle Q(x) \rangle_{(x)} \\ &= \frac{\langle Q(x + \Delta x) e^{-\Delta U/k_B T} \rangle_{(x)}}{\langle e^{-\Delta U/k_B T} \rangle_{(x)}} - \langle Q(x) \rangle_{(x)}. \end{aligned} \quad (15)$$

This expression converges more rapidly since the fluctuations in  $\langle Q(x + \Delta x) \rangle$  and  $\langle Q(x) \rangle$  cancel each other because they are taken from the same trajectory. Eq. 15 is used to compute the profile of several different quantities: the distortion of the average channel-water dipole relative profile in the presence of a  $\text{Na}^+$  ion  $Q(x) = \mu(x) = \sum_i q_i x_i$ ; the average ion-channel interaction energy relative profile  $Q(x) = U_{i,c}(x)$ ; the average ion-water interaction energy relative profile  $Q(x) = U_{i,w}(x)$ ; the average total interaction energy relative profile  $Q(x) = U(x)$ . The latter is necessary to estimate the relative entropy profile  $S(x)$  (as described below).

A similar perturbation technique can be used to examine the effects

of a modification of the interaction parameters on a free energy profile. In the analysis of complex systems with many interactions this is a useful tool to estimate the sensitivity of the results to the parameters of the empirical energy function. Using arguments similar to those leading to Eqs. 4, 13, and 15, we can write

$$\begin{aligned} \Delta \mathcal{W}(x \rightarrow x + \Delta x) &= \mathcal{W}(x + \Delta x) - \mathcal{W}(x) \\ &= -k_B T \ln \left[ \frac{\langle e^{-\Delta U_1/k_B T} e^{-\Delta U_2/k_B T} \rangle_{(x)}}{\langle e^{-\Delta U_2/k_B T} \rangle_{(x)}} \right], \end{aligned} \quad (16)$$

where  $\Delta U_1 = U' - U$  is the difference between the total modified potential energy  $U'$  (with modified parameters) and the total reference potential energy  $U$ ; and  $\Delta U_2 = U'(x + \Delta x) - U'(x)$  is the change in interaction energy induced by a small displacement of the ion from position  $x$  to position  $x + \Delta x$  using the modified energy function  $U'$ . This term is analogous to  $\Delta U$  appearing in Eq. 4, except that here it is calculated using a potential function that is not the one ( $U$ ) employed to generate the molecular dynamics trajectory. The energy difference  $\Delta U_1$  could result from a modification of the ion-peptide interaction, or from changes in the peptide–peptide, water-peptide, or water–water interactions. Eq. 16 is a special case of Eq. 15 with  $Q(x) \equiv \exp(-\Delta U_2/k_B T)$ .

## Computational details and simulation procedure

All calculations with the periodic  $\beta$ -helix system were performed with the CHARMM program (39), appropriately modified to incorporate the ion-peptide potential Eqs. 1 and 2. The IMAGE generation facility in CHARMM was used to impose the periodic boundary conditions. To implement Eq. 4, a molecular dynamics simulation of the full system with the ion constrained at a given  $x$  is generated and stored in a file. Subsequently, this file is read and the ion-system interaction energy is calculated for the ion at  $x$  and at  $x \pm \Delta x$  while keeping all other coordinates (including the  $y$  and  $z$  coordinates of the ion) equal to the values obtained in the trajectory. Other energy terms (water–water, water-peptide, and peptide–peptide interactions) do not appear in the energy difference  $\Delta U$  in Eq. 4 (49). The average in Eq. 5 is obtained by summing over all the stored coordinates of the trajectory. The equilibrium average represents the integration over all degrees of freedom in the system other than  $x$ , the motion of the ion in the cross-section of the channel perpendicular to the axis is included. From this procedure the relative potential of mean force along  $x$  is defined up to an arbitrary constant (the constant sets the free energy of the initial  $x$  to zero). The rate of convergence expected from Eq. 16 depends on the size of  $\Delta x$ . One criterion is to require that the configurational region covered by the simulation with the reference system have significant overlap with the configurations expected to be dominant in the perturbed system. In practice, the perturbations have to be relatively small to obtain rapid convergence. Trial and error calculations with the free energy simulation technique showed that good results can be obtained only if  $\Delta x$  is smaller than 0.1 Å. Increasing  $\Delta x$  beyond this limit gives rise to a spurious “repulsive-like” response of the environment and always produces large positive free energy changes. This behavior is due to the lack of overlap between the configurations with the ion at  $x$  and those where the ion is fixed at  $x + \Delta x$ . The maximum distance  $\Delta x$  is much smaller than the one used by Tobias and Brooks in a liquid argon simulation (27), ( $\Delta x = 0.2$  Å). This difference is probably due to the large electrostatic forces and the extreme confinement of the present system. It was found necessary to carry out eight simulations to determine the free energy profile along the helix for  $x$  between 0.0 and 1.55 Å. This gave a perturbation distance  $\Delta x$  equal to  $(1/6) \times 1.55$  Å. In practice, the free energy difference was computed for smaller perturbed positions ( $-\Delta x$ ,

$-\Delta x/2$ ,  $+\Delta x/2$  and  $+\Delta x$ ) around each simulation to obtain a smoother profile. A ninth simulation, which should be equivalent to the first one by symmetry, was calculated to determine the statistical convergence. Trials with the mean force integration method showed that Eq. 8 does not give results equivalent to Eq. 6 using only the average forces evaluated at the simulations. The inaccuracy is due to the fact that the integral in Eq. 8 is not well approximated by a discrete sum of eight values of the integrand corresponding to the eight actual simulations. Good agreement with Eq. 6 is obtained by including the value of the force evaluated at location between the actual simulations. The average forces was calculated in the neighborhood of the eight simulations using Eq. 13 for  $\Delta x = (\gamma_{32}) \times 1.55 \text{ \AA}$ . The integration along the  $x$  coordinate was then performed using the trapezoidal rule.

The free energy simulation protocol (after the initial stages of equilibrium described above) consisted of (a) a 25-ps trajectory is generated with the ion constrained at  $x$  and the free energy difference calculated for  $-\Delta x$ ,  $-\Delta x/2$ ,  $+\Delta x/2$ , and  $+\Delta x$ ; (b) the ion is displaced by  $x + 2\Delta x$  ( $0.19 \text{ \AA}$ ) along the  $x$  axis for the next simulation; (c) a short energy minimization is applied to the water and the channel atoms surrounding the ion (ABNR) (39) to remove local strains and the system is equilibrated during 5 ps of molecular dynamics with the ion constrained at the new  $x$  position; (d) the cycle is repeated starting with step a. Finally, all the free energy differences are pieced together using Eq. 6 to generate the free energy profile  $\mathcal{W}(x)$ . The various ensemble averages were evaluated using configurations separated by 0.02 ps. For the dynamics of the atoms others than hydrogens the Langevin equation (47) was used with frictional drag  $\xi$  and a weak random force, corresponding to a relaxation time  $m/\xi = 0.014 \text{ ps}$ . This insures proper thermalization for the configurational sampling and a stable bath temperature of  $300^\circ\text{K}$  in this relatively small system; (the relaxation time corresponds to the bulk diffusion constant for water,  $2.1 \times 10^{-5} \text{ cm}^2/\text{s}$ ). It should be pointed out that too large a frictional drag might decrease the effective diffusion constant and slow down conformational transformations required for structural equilibrations and convergence. To generate the proper ensemble and obtain the correct averaging, the center of mass of the helix was constrained to  $x = 0$  but the helix was free to move in the  $y$  and  $z$  directions. All constraints, namely on the ion, the helix center of mass and the N-H bonds were applied using the SHAKE algorithm (50). No other constraints were applied on the channel to maintain the  $\beta$ -helix conformation, in contrast to other studies (40).

The free energy difference between  $\text{Na}^+$  and  $\text{K}^+$  was calculated by transforming the values of the  $A^{(8)}$  and  $B^{(6)}$  coefficients of the  $\text{Na}^+$  ion to those for  $\text{K}^+$  ion. Two ions with intermediate parameter values, obtained from a linear interpolation of the  $A^{(8)}$  and  $B^{(6)}$  coefficients of  $\text{Na}^+$  and  $\text{K}^+$ , were used. The helix system was equilibrated during 5 ps for each intermediate ion, after which a 25-ps trajectory was generated for the averaging. The position of the ion was constrained at a constant  $x$  position corresponding to the minimum of the free energy profile during the transformations. A group-by-group based cut-off of  $12 \text{ \AA}$  was used with a smooth switching region of  $4 \text{ \AA}$ . The integration time step was 0.001 ps.

## RESULTS AND ANALYSIS

### Ion free helix

The average dihedral angles obtained from the molecular dynamics simulation of the water-filled helix are very similar to those of the energy minimized empty helix (see Table 1). The mean square dihedral angle fluctuations are similar to those reported in a vacuum normal

modes analysis (51) and in a molecular dynamics simulation of the solvated gramicidin channel. Association of the water molecules with the backbone is controlled by the accessibility of the helix atoms. During the simulations, the water molecules remained in an essentially linear structure, hydrogen bonding to one another and to the carbonyl oxygens of the helix. No association of the water molecules with the amide groups of the backbone is observed because they are poorly accessible for hydrogen bonding. After 116 ps a transition occurred in  $\sim 1 \text{ ps}$  and the orientation was inverted. No significant difference in the overall water motion was observed in the two segments of the trajectory, so the statistical averages were calculated using the whole 250 ps trajectory. Such linear arrangements of water molecules in the gramicidin dimer channel and their concerted transitions have been observed and reported previously (40, 52).

The accessibility of the carbonyl and amide groups of the backbone for hydrogen bonding with the water molecules is consistent with the librational fluctuations of the  $\beta$ -helix (51, 53). The water molecules hydrogen bond with the carbonyl oxygens with no net preference for L or D amino acids. This is due to the fact that the periodic  $\beta$ -helix is fairly regular in the absence of end effects causing all the carbonyl oxygens to have similar accessibility from the inside of the channel.

The free energy profile of the water oxygens, extracted from the water-filled ion free helix simulation, through the average oxygen density profile  $\langle \rho_{\text{water}}(x) \rangle$ ,

$$\mathcal{W}_{\text{water}}(x) = \mathcal{W}_{\text{water}}(x_0) - k_B T \ln \left[ \frac{\langle \rho_{\text{water}}(x) \rangle}{\langle \rho_{\text{water}}(x_0) \rangle} \right] \quad (17)$$

is shown in Fig. 3. The oxygen density profile from the simulation indicates that the water molecules have a tendency to hydrogen bond spontaneously to the backbone carbonyl oxygens. However, the effective free

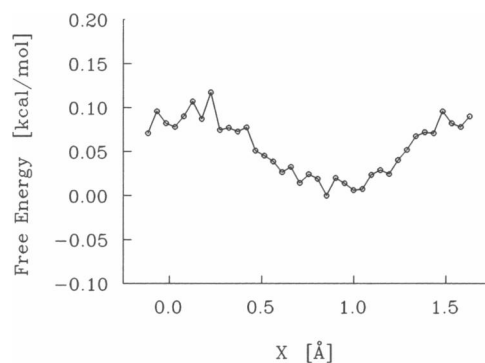


FIGURE 3 Water oxygen free energy profile extracted from the oxygen density in the water-filled helix simulation from Eq. 17.

energy barrier along the axis is only 0.1 kcal/mol, indicating that the perturbation of the uniform water spacing, though clearly there, is a very small effect. As we show below, this effect does play an important role in the ion free energy profile. The variation in water oxygen density is due to the nonhomogeneous distribution of the carbonyl oxygen along the helix axis; i.e., the accumulation of water in the range 0.8–1.2 Å in Fig. 3 is due to the larger linear density of carbonyl oxygens in this region. For the results shown in the figure, the carbonyl oxygen appear in the order 13, 18, 15, 20, 17, 22 from the NH<sub>2</sub>- to the COOH-terminus along the helix axis. This gives rise to a periodic sequence of favorable specific locations separated by 1.55 Å (see also Fig. 7 for the distribution of carbonyl oxygens).

## Free energy profile

The results obtained from the potential of mean force simulations for Na<sup>+</sup> and K<sup>+</sup> ions with Eq. 4 are shown in Fig. 4. For Na<sup>+</sup>, minima exist near  $x = 0$  and  $x = 1.5$ , separated midway by an energy barrier of 4.5 kcal/mol. The free energy profile of K<sup>+</sup> varies much less than the

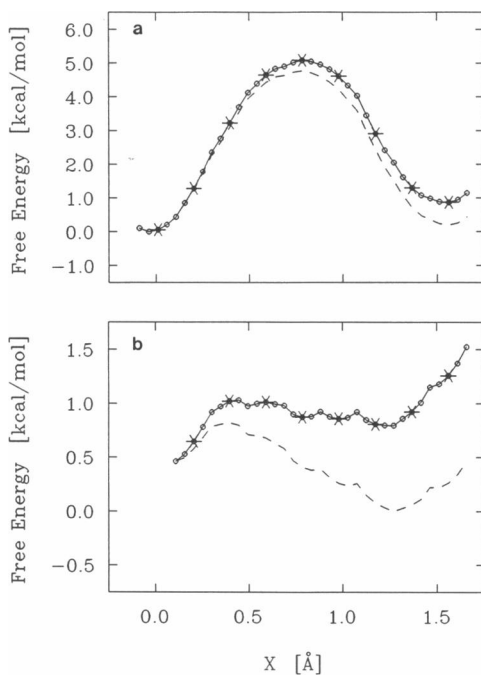


FIGURE 4 Free energy profile of Na<sup>+</sup> (a) and K<sup>+</sup> (b) ions as obtained from the perturbation technique. The “\*” indicate the locations of the simulations (nine for Na<sup>+</sup> and eight for K<sup>+</sup>) and the “o” represents the positions where free energy differences were computed by Eq. 5. An hysteresis of 0.8 kcal/mol and 1.0 are observed for Na<sup>+</sup> and K<sup>+</sup>, respectively. The linearly corrected profile are plotted with dashed lines.

one calculated for Na<sup>+</sup> ion and the observed energy barrier is ~1.0 kcal/mol. The weaker binding site is slightly displaced relative to Na<sup>+</sup> ion. In the periodic helix the potential of mean force for Na<sup>+</sup> along the axis is made up of a sequence of well-defined binding sites and energy barriers separated by 1.55 Å. For K<sup>+</sup>, the weaker binding sites are slightly displaced relative to Na<sup>+</sup>. The relation of these results to the free energy profile in the finite gramicidin channel is discussed in a subsequent paper.

For Na<sup>+</sup> ion a slight discrepancy of 0.7 kcal/mol is present between the value of the potential of mean force at  $x_0$  and at  $x_0 + \Delta L$ , although the periodicity of  $\mathcal{W}(x)$  is clear. Such hysteresis, violating the periodicity of the profile, is caused by insufficient equilibration and sampling for the various values of  $x$ . Because the simulations were carried out with sequentially increasing values of  $x$ , it is likely that inadequate equilibration introduced a drag in the opposite direction. Increasing the equilibration period to 10 ps and using the remaining 20 ps for averaging reduced the hysteresis to 0.2 kcal/mol. Assuming that a constant dragging force acting in the  $-x$  direction produces a spurious linearly increasing potential we can correct the calculated values to obtain a periodic result. The hysteresis was rectified using a linear correction given by  $-\Delta_{\text{error}}(x - x_0)/\Delta L$ , where  $\Delta_{\text{error}}$  is  $[\mathcal{W}(x_0 + \Delta L) - \mathcal{W}(x_0)]$ . This procedure results in a uniform distribution of the error over the interval  $[x_0, x_0 + \Delta L]$ . Removing the “dragging linear potential” from the calculated potential has little effect on the form of the profile and the energy barrier, as shown in Fig. 4. For K<sup>+</sup> the hysteresis is somewhat larger and the profile in Fig. 4 b has been rectified by a linear correction for a hysteresis of 1.0 kcal/mol. All the subsequent results were rectified by a corresponding hysteresis correction.

## Structural analysis of ion translocation

The free energy profile of Na<sup>+</sup> indicates a sequence of well-defined binding sites and transition states; there is one such binding site for every two carbonyl oxygens. As a first step in the analysis of the free energy barrier, a search was made to find the nearest neighbors of the Na<sup>+</sup> in the two equivalent binding sites and at the intervening barrier. The average distances between the Na<sup>+</sup> and the nearest carbonyl oxygens are shown in Fig. 5. The most important contacts made by the ion are illustrated schematically in Figs. 6 and 7 and plotted in Figs. 8 (stereo view) and 9. There are four carbonyl oxygens and two water molecules in close contact with the ion in each binding site. They form a tight solvation structure (see Fig. 6 and the analysis of the cage structure below). The solvation structure around the ion

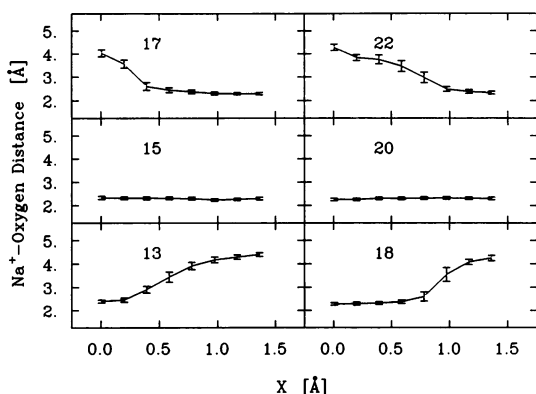


FIGURE 5 Structural information about the average distances between the  $\text{Na}^+$  ion and the nearest carbonyl oxygens. The vertical lines represent the rms fluctuations.

is transformed in a continuous fashion as the ion moves from a binding site through the transition state to the adjacent binding site. During the transition the ion remains in close contact with two of the four carbonyls involved in the first binding site and the two other carbonyls are replaced by two new carbonyls. In the first well examined ( $x = 0$ ), the  $\text{Na}^+$  ion makes close contact with L-carbonyl 13 and L-carbonyl 15 (pointing toward

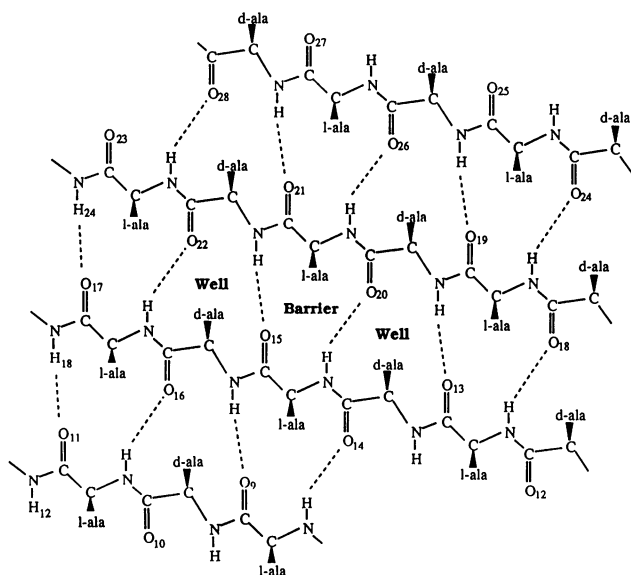


FIGURE 6 Schematic representation of the ion translocation with the successive binding sites and transition states represented for the left-handed  $\beta$ -helix (the mirror image of the diagram would describe the translocation for a right-handed  $\beta$ -helix). The figure is obtained by cutting open the  $\beta$ -helix along its axis and lying the structure flat on a plane. The ion always interact with the four carbonyl oxygens nearest in distance along the channel axis (see also Fig. 7).

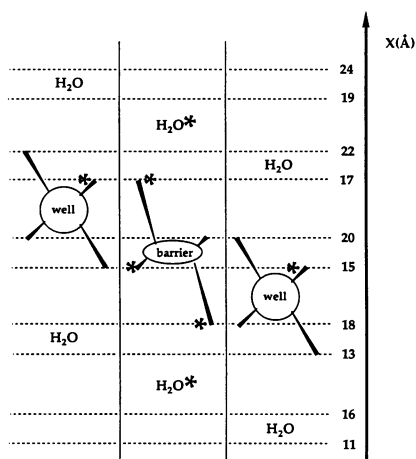
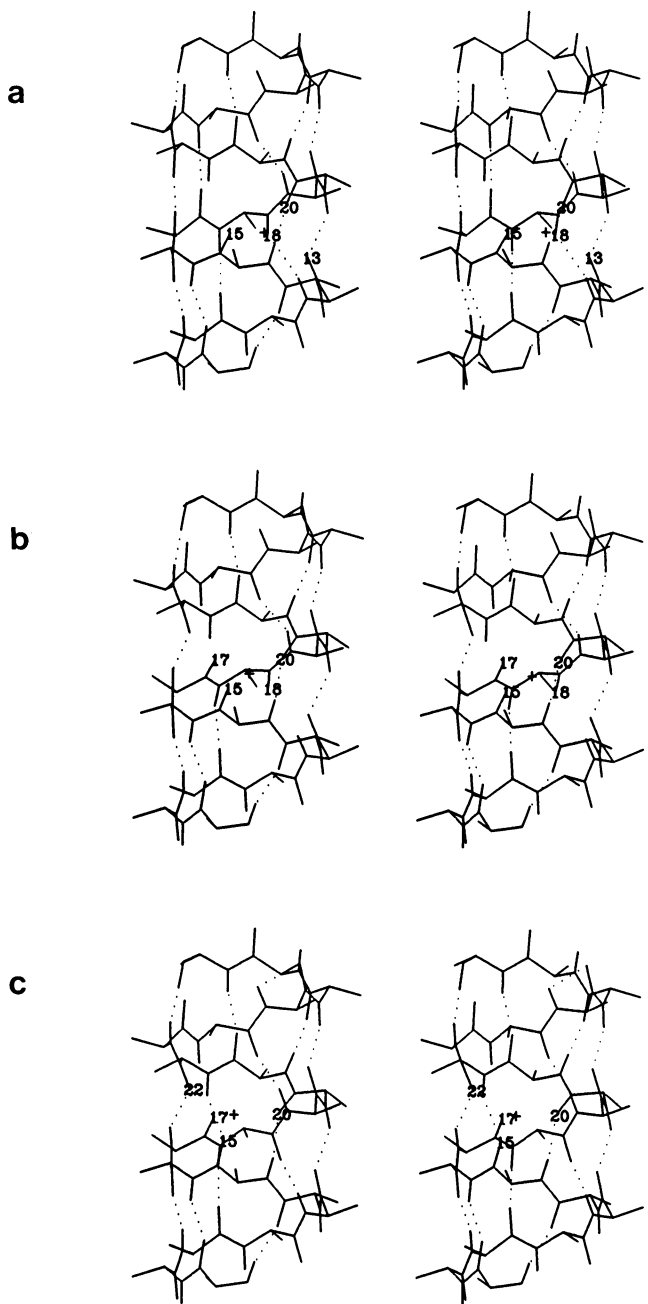


FIGURE 7 Schematic representation of the ion translocation with the two nearest water molecules in the successive binding sites and transition states along the channel axis. The distance along the helix axis is 0.52 Å between carbonyl 15 and 20 and is 1.03 Å between carbonyl 20 and 17. The other distances can be determined from the periodicity. The ion always interact with the four carbonyl oxygens nearest in distance along the channel axis. The position of the water molecules relative to the peptide is indicated by a “ $\text{H}_2\text{O}$ .” The water-peptide and peptide-peptide hydrogen bonds lost when the ion is at the transition state are indicated by a “★”. When  $\text{Na}^+$  ion is in the first energy well, making contact with carbonyl 13, 15, 18, and 20, the first water molecule is hydrogen bonded to carbonyl 11 and the second water is hydrogen bonded to carbonyl 17. As the ion moves to the second binding site these water carbonyl hydrogen bonds are broken and reformed with carbonyls number 13 and 19. The hydrogen bonds are very stable as can be observed in Fig. 11 from the small ellipsoids of fluctuations found for the water hydrogens. A well defined water-ion complex can be observed in the binding site.

the COOH-terminus) and D-carbonyl 20 and D-carbonyl 18 of the next turn (pointing toward the  $\text{NH}_2$ -terminus). The transition state occurs when the ion moves one residue toward the  $\text{NH}_2$ -terminus (0.75 Å). An adjacent binding site is found two residues further toward the  $\text{NH}_2$ -terminus, where the ion is in contact with L-carbonyl 15 and 17, and D-carbonyl 20 and 22. At the transition state, the ion remains in close contact with two of the four carbonyls of the nearest binding sites, the contact with the remaining two carbonyls (13 and 22) is essentially lost. The ion contact with two water oxygens is maintained through the entire transition with an average ion-oxygen distance of 2.32 Å.

The average “cage” structure of the binding site was calculated in a local reference frame from 25 ps of the simulation to remove the transverse fluctuations of the helix (these fluctuations are on the order of 0.6 Å). In this procedure, the coordinates of the cage atoms are reoriented for each configuration to minimize the root-mean square (rms) deviation from an initial structure. The result is the average “local” structure from the view



**FIGURE 8** Stereo stick representation of  $\text{Na}^+$  ion translocation with the successive binding sites and transition states illustrated for the left handed  $\beta$ -helix. In the first well (*a*), the ion makes contact with carbonyl oxygens 15, 20, 13, and 18. Only carbonyl oxygen 15 loses its hydrogen bond in the helix. At the transition state (*b*), the ion makes contact with 15, 17, 18, and 20. Carbonyl 15, 17, and 18 lose their hydrogen bond in the helix. In the next well (*c*), the ion makes contact with carbonyl oxygens 15, 17, 20, and 22. Only carbonyl oxygen 17 loses its hydrogen bond. For the sake of clarity, these structures were obtained by energy minimization of the helix constraining the ion at the three successive positions.

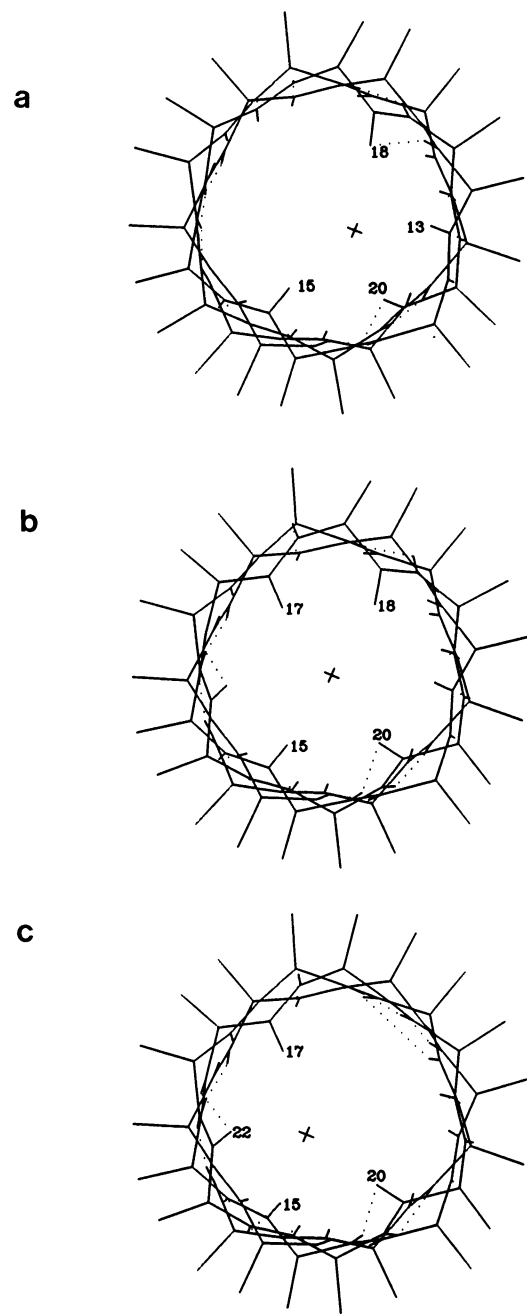


**FIGURE 9** Cross-section of the left handed  $\beta$ -helix during  $\text{Na}^+$  ion translocation along the axis (see also Fig. 8). In the first well (*a*), the ion makes contact with carbonyl oxygens 15, 20, 13, and 18. At the transition state (*b*), the ion makes contact with 15, 17, 18, and 20. Carbonyl 15, 20 are on opposite side from carbonyls 17 and 18. In the next well (*c*), the ion makes contact with carbonyl oxygens 15, 17, 20, and 22.

point of the ion. This consists of the four nearest  $\text{C} = \text{O}$  and two water molecules. The average binding site structure for  $\text{Na}^+$  is shown in Fig. 10 and the average coordinates are given in Table 5. The six ligands totally

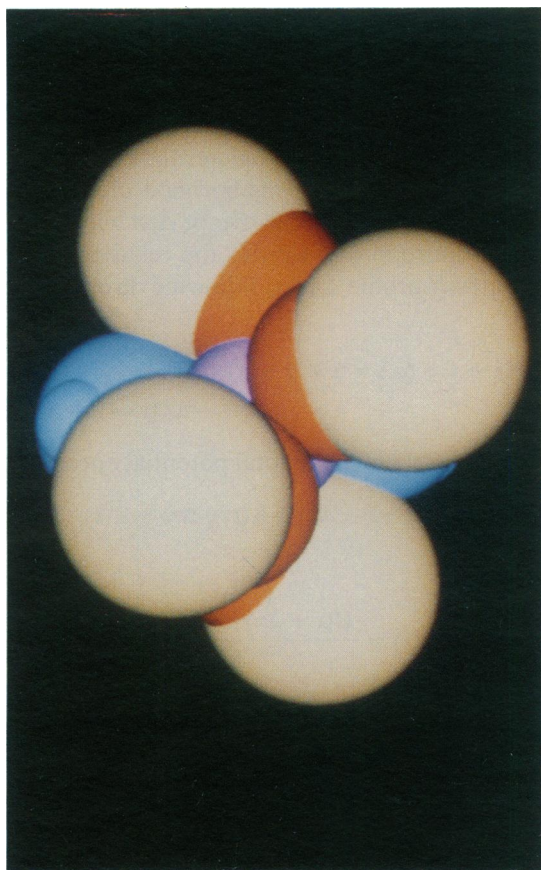


FIGURE 10 Space filling representation of the  $\text{Na}^+$  ion surrounded by the four nearest  $\text{C}=\text{O}$  carbonyl and the two nearest water molecules for a total of six ligands in the binding sites. The picture was made with QUANTA.

surround the ion to provide efficient solvation with very tight contacts. The solvation shell has the structure of a distorted octahedron. The results are similar for  $\text{K}^+$  ion, though the distances are larger. The local fluctuations relative to the average structure are shown in Fig. 11 *a* for  $\text{Na}^+$ . The fluctuation ellipsoids are small, indicative of a tight structure solvating the ion. The average structure of the transition state and its fluctuations were calculated in the same way. The fluctuation ellipsoids are shown in Fig. 11 *b* and indicate larger fluctuations for most of the atoms.

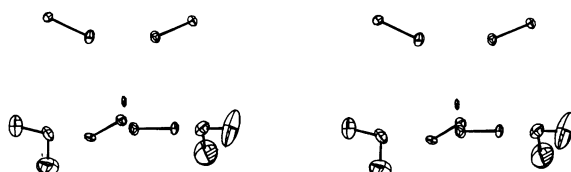
The solvation of the ion in the binding site and transition state induces some local distortion of the helix. The average  $\phi$  and  $\psi$  dihedral angles and the rms fluctuations are shown in Fig. 12 for an ion located at the origin. The dotted lines in Fig. 12 indicate the range of the dihedrals fluctuations of the water-filled simulation (i.e., in the absence of the ion). The average position of most dihedrals lies between the normal fluctuations and

TABLE 5 Solvation structure around  $\text{Na}^+$

Residue	Atom	Coordinates ( $\text{\AA}$ )		
		x	y	z
$\text{Na}^+$		0.00	0.00	0.00
L-Ala <sup>15</sup>	O	-1.04	1.79	-0.98
	C	-2.14	2.33	-1.11
L-Ala <sup>17</sup>	O	-0.20	-2.23	-0.45
	C	-1.26	-2.79	-0.70
D-Ala <sup>20</sup>	O	0.12	1.65	1.58
	C	1.08	1.99	2.28
D-Ala <sup>22</sup>	O	0.78	-0.14	-2.18
	C	1.84	0.21	-2.69
$\text{H}_2\text{O}$	O	2.15	-0.56	0.50
	H	3.01	-0.40	0.26
	H	2.22	-1.12	1.20
$\text{H}_2\text{O}$	O	-2.11	-0.26	0.90
	H	-2.18	-0.14	1.78
	H	-2.88	-0.68	0.71

the influence on the fluctuations is small. Only the dihedral angles of the four carbonyls making contact with the ion are strongly perturbed, although there is also a clear longer range response of the helix that is correlated with the ion position.

a



b

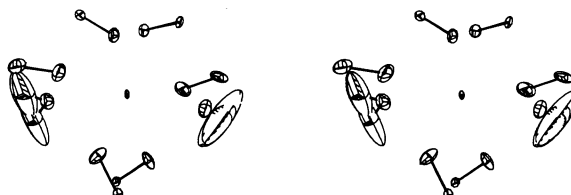


FIGURE 11 Fluctuations ellipsoids of  $\text{Na}^+$  in the  $\beta$ -helix. (a)  $\text{Na}^+$  ion in a binding site. Carbonyls number 13 (top left), 15 (bottom left), 18 (bottom right), and 20 (top right) and the two nearest water molecules are shown. (b)  $\text{Na}^+$  ion in at transition state. Carbonyls number 17 and 18 (bottom), 15 and 20 (top), 13 and 22 (left and right) and the two nearest water molecules are shown. The drawings were made with CHEMGRAF.

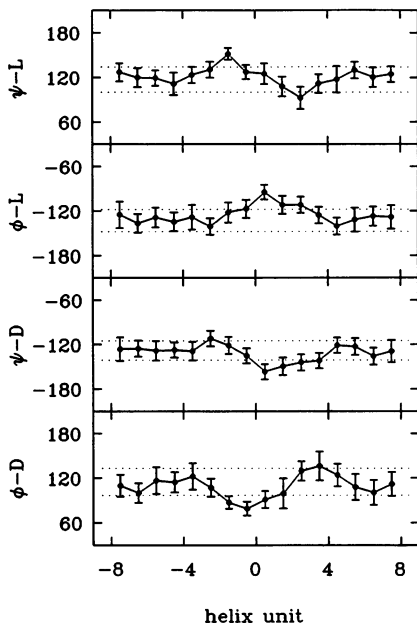


FIGURE 12 Backbone  $\phi$   $\psi$  dihedral angles of the channel in presence of the  $\text{Na}^+$  ion in the first binding site (the nearest residue to the ion is labeled 0). The dotted lines represent the range of the rms fluctuations in the ion-free simulation.

As a test of the convergence of the statistical averages in the simulations, the average structure of the binding site computed from the first and the last simulations were compared for  $\text{Na}^+$  ion. From the periodicity of the helix they should be identical. The average rms deviation between the two structures is  $\approx 0.09 \text{ \AA}$ , i.e., they are virtually identical. The comparison of the structures around  $\text{Na}^+$  and  $\text{K}^+$  shows that they have the same form. The average rms deviation between the  $\text{Na}^+$  and  $\text{K}^+$  average binding site cage structure is  $\approx 0.39 \text{ \AA}$ . This difference is due to the larger nonbond distances associated with the difference in  $\text{Na}^+$  and  $\text{K}^+$  parameters (see Tables 2–4).

## Thermodynamic decomposition

To gain more insight in the origin of the potential of mean force and of the transition state barrier the free energy profile was decomposed into its entropic  $\mathcal{S}(x)$  and average total internal potential energy  $\mathcal{E}(x)$  contributions (average internal energy is more appropriate than enthalpy here because all evaluations and thermodynamic derivatives are done at constant volume and not at constant pressure). The entropic contribution to the free energy profile, i.e.,  $-T\mathcal{S}(x)$ , is defined from the known thermodynamic relation (47),

$$\mathcal{W}(x) = \mathcal{E}(x) - T\mathcal{S}(x), \quad (18)$$

in terms of the temperature derivative:

$$-T\mathcal{S}(x) = T \left( \frac{\partial \mathcal{W}(x)}{\partial T} \right)_V. \quad (19)$$

Eqs. 18 and 19 can be used to determine the increments  $\Delta\mathcal{W}$ ,  $\Delta\mathcal{S}$  and  $\Delta\mathcal{E}$  in the neighborhood of a simulation. Evaluating the partial derivative of  $\Delta\mathcal{W}$  with respect to the temperature in Eq. 4 yields the relative increments of the entropy profile  $\Delta\mathcal{S}(x)$  following directly from Eq. 18

$$-T \Delta\mathcal{S}(x \rightarrow x + \Delta x) = \Delta\mathcal{W}(x \rightarrow x + \Delta x) - \Delta\mathcal{E}(x \rightarrow x + \Delta x), \quad (20)$$

with the increments in the total potential energy,

$$\Delta\mathcal{E}(x \rightarrow x + \Delta x) = \mathcal{E}(x + \Delta x) - \mathcal{E}(x), \quad (21)$$

given by

$$\Delta\mathcal{E}(x \rightarrow x + \Delta x) = \frac{\langle U(x + \Delta x) e^{-\Delta U/k_B T} \rangle_{(x)} - \langle U(x) \rangle_{(x)}}{\langle e^{-\Delta U/k_B T} \rangle_{(x)}} - \langle U(x) \rangle_{(x)}. \quad (22)$$

This equation is a special case of Eq. 15. The average ion-channel and ion-water interaction energy profiles were also calculated from Eq. 15 with the interaction energy  $U_{i-c}(x)$  and  $U_{i-w}(x)$  replacing  $U(x)$ . As can be noticed in Eqs. 20 and 22, the variation in the total energy, and the entropy, involve averages of the total potential energy and the difference in the total potential energy of the system along the reaction coordinate. This is in contrast with the expression for the free energy difference Eq. 4 which depends only on the ion-system interaction energy (49). This fact makes Eq. 22 much more difficult to evaluate accurately than Eq. 4. The total potential energy has large fluctuations during the simulations and the computation of the energy and entropy converge more slowly than the free energy profile. An alternative approach uses the finite difference analogue of Eq. 19 (54). Eqs. 20 and 22 have not been used previously to compute energy and entropy profile along a reaction coordinate. The two approaches are formally identical but could differ in their convergence rate.

The average ion-water, ion-channel, and total potential energy profiles are shown in Fig. 13. The entropic contribution to the free energy profile, calculated from Eq. 20, is shown in Fig. 14. An hysteresis on the order of  $+9.9$  and  $-9.2 \text{ kcal/mol}$  was found in computing  $\mathcal{E}(x)$  and  $-T\mathcal{S}(x)$ , respectively; these were rectified by distributing the error uniformly over the whole interval using a linear correction as described above. The larger errors are indicative of the much slower convergence than for the free energy, for which the hysteresis is only  $+0.7 \text{ kcal/mol}$ . In spite of the uncertainty due to the

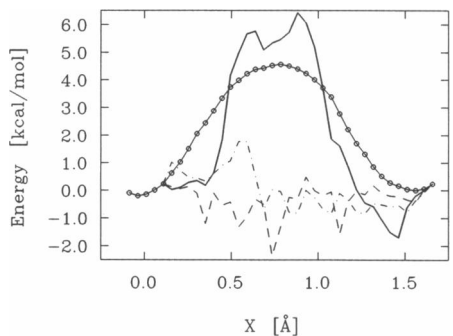


**FIGURE 13** Energy decomposition of the potential of mean force of  $\text{Na}^+$  ion. The relative total energy profile  $S(x)$  (solid line) was calculated from Eq. 22 after rectified linearly to remove a hysteresis of +9 kcal/mol. The relative ion-channel (dashed line) and ion-water (dot-dashed line) interaction energy were calculated from Eq. 15. The free energy profile  $W(x)$  (solid line with circles) is shown for comparison.

large statistical errors the results are suggestive. The activation free energy barrier is dominated by the energy contribution, except near the minimum ( $x = 0.0\text{--}0.3 \text{ \AA}$  and  $1.2\text{--}1.5 \text{ \AA}$ ) where the entropy contributes up to 2 kcal/mol and is dominant; between 0.3 and 1.2 Å, the energy makes the primary contribution. In the region of the maximum, the entropy is slightly stabilizing; i.e., an increase in entropy at the top of the barrier compensates for the loss of favorable interaction energy by ~2 kcal/mol.

The entropic stabilization, resulting from an increase in the fluctuations, appears to be local in character as it is evident in the ion-ligand distance plots (Fig. 5) and the larger fluctuation ellipsoids at the transition state (Fig. 11, *a* and *b*). Thus, the motion of a  $\text{Na}^+$  ion from one binding site to the next is aided by an increase in fluctuations at the transition state. Similar mechanisms

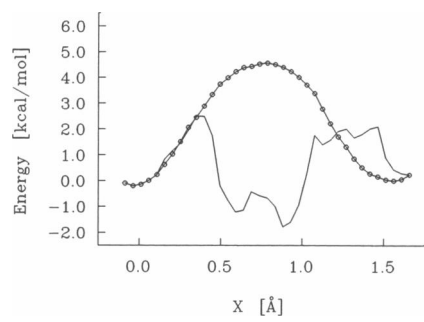


**FIGURE 14** Relative entropic contribution  $-TS(x)$  (solid line) to the free energy profile of  $\text{Na}^+$  ion obtained from Eqs. 20 and 22. The curve was rectified linearly to remove a hysteresis of -8 kcal/mol. The free energy profile  $W(x)$  (solid line with circles) is shown for comparison.

have been reported for other ionic systems (55). In a flexible system with strong associative forces it is reasonable to expect that the larger distortion at the transition state would be accompanied by an increase in fluctuations as the system tries to adapt to the transition state. This observation is in contradiction with the conclusion of Brickmann and Fisher (56) who assumed that the entropic contribution to the activation free energy is unfavorable. Their assumption appears to result from a physical picture based on a rigid channel. They simulated (57) a gramicidinlike helix using a peptide libration frequency of  $213 \text{ cm}^{-1}$  which is appropriate for the out-of-plane motion of the carbonyl oxygen, and is not the dominant mechanism for the C=O dipole reorientation (51). The frequencies involved are in the range of  $75\text{--}150 \text{ cm}^{-1}$  (51). Normal mode study of the gramicidin A dimer (51) has shown that models based on totally (23, 24) or nearly (56–58) rigid structure do not give a realistic representation of the channel.

The average ion-water and ion-channel interaction energies do not contribute significantly to the activation energy barrier. The total internal potential energy can be decomposed into direct ion-water and ion-channel interaction energies, and a “cavity formation” contribution arising from changes in the average peptide-peptide, peptide-water and water-water interaction energy (49). The energy at the transition state relative to the minimum must therefore arise from a loss of interactions of the host system; i.e., although the ion-water and ion-channel interaction energy make the dominant contribution to the free energy of solvation (~100 kcal/mol for  $\text{Na}^+$ ), they remain essentially constant inside the periodic helix. This is due to the fact the local solvation structure around the  $\text{Na}^+$  ion does not vary significantly along the helix axis. It is dominated by the strong interactions with the nearest ligands, four carbonyls and two water molecules, whose distance from the ion remain essentially constant (the distances are 2.30 to 2.32 Å on the average). It is the weaker interactions (peptide-peptide, peptide-water and water-water) which adjust to the ion motion and store the strain energy. This is analogous to a strained coupled oscillator system in which more energy is stored in the softer spring. This observation disagrees with the assumption that the ion-channel interaction energy is responsible for the free energy profile and the channel selectivity (6, 23).

## Mean force decomposition

The separate contribution of the water molecules and the channel to the relative potential of mean force are calculated using Eqs. 9–11. The results of these calculations are shown in Fig. 15. The decomposition of  $W(x)$

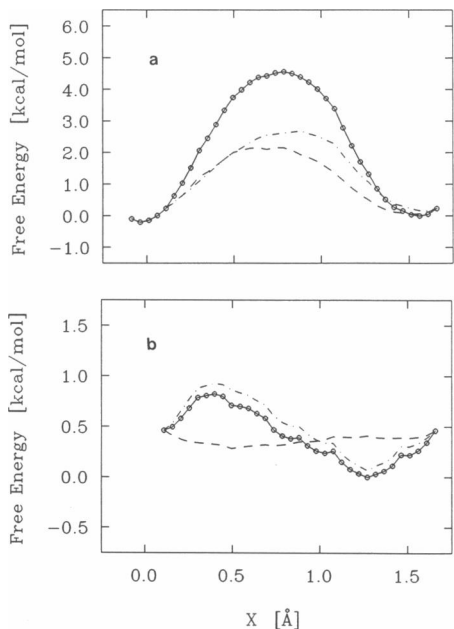


**FIGURE 15** Water (dot-dashed line) and channel (dashed line) contributions to the free energy profile of  $\text{Na}^+$  (*a*) and  $\text{K}^+$  (*b*) ion from the mean force decomposition.

into water and channel mean force contributions is essentially different from the average ion-channel and ion-water interaction energy decomposition shown in Fig. 13. The average interaction energy is only one of the contributions to the potential of mean force, which also contains a “cavity formation” term, arising from the potential energy of deforming the “host” system in which the ion is inserted, and an entropic contribution, arising from the change of fluctuations in the host system (49). The essential difference between the potential of mean force  $\mathcal{W}(x)$  and the average interaction energy  $\langle U(x) \rangle$  is not always made explicit (23, 24, 58). As can be seen from Fig. 15, for both  $\text{Na}^+$  and  $\text{K}^+$  ions the water molecules contribute significantly to the total potential of mean force. The water molecules contribute 2.5 kcal/mol to the 4.5 kcal/mol free energy barrier of  $\text{Na}^+$  ion, and represent most of the 1.0 kcal/mol free energy barrier of  $\text{K}^+$  ion. Further analysis indicates that these contributions can be understood in terms of localized interactions of the ion with the channel or water nearest neighbors (see below). As was demonstrated in the previous section, the presence of an ion induces relatively localized structural changes and the translocation from one binding site to the next is achieved without loss of favorable contact with the carbonyls or water ligands. Comparison of the mean force contribution of the two nearest water molecules and the six closest carbonyls with the value from the entire system shows that the free

energy barrier arises essentially from very localized interactions. These structural and energetical results indicate that the free energy profile of  $\text{Na}^+$  and  $\text{K}^+$  ions may be understood from the interactions with the nearest neighbors and do not depend on global or more distant effects involving changes in the helix conformation. We now proceed to analyze the structural origins of the water and channel contributions.

The water mean force contribution to the free energy profile of the ions can be understood in terms of the periodic helical structure. In the absence of any ion, the water oxygens have a spontaneous tendency to occupy specific positions in the helix, i.e., in the wells of the water oxygen free energy profile as shown in Fig. 3. The positioning of the water oxygen free energy profile relative to the ions free energy profile plays an important role. The presence of an ion perturbs the periodic arrangement of the water molecules in the helix. The large difference between the water mean force on  $\text{Na}^+$  and  $\text{K}^+$  arises from their difference in size in relation to the helix periodicity. This is illustrated schematically in Fig. 16. During the simulation, the average distance between the  $\text{Na}^+$  ion and the two nearest-neighbor water oxygens is 2.32 Å, whereas it is 2.71 Å in the case of  $\text{K}^+$  ion, just the 0.39 Å difference in structure mentioned earlier. The 2.23 Å value for  $\text{Na}^+$  is such that the waters ahead and behind the ion are in favorable sites. Because  $\text{Na}^+$  is at a maximum of the water free energy (see Fig.

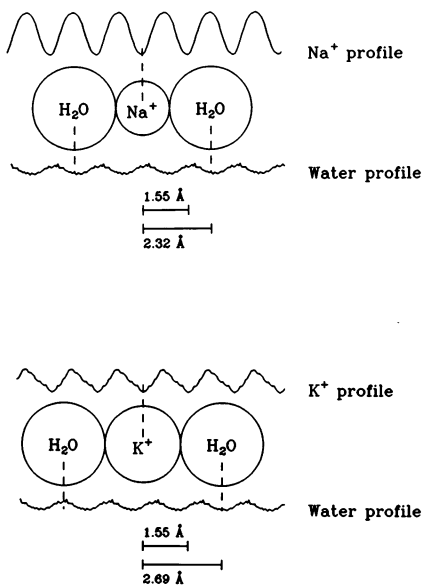


**FIGURE 16** Schematic representation of the periodic free energy profile of  $\text{Na}^+$  (*a*)  $\text{K}^+$  (*b*) ions relative to the water oxygen profile. The water oxygen profile has been magnified by 10 relative to the ion profile for clarity. No translation or scaling were applied to any of the profiles in the *x* direction.

16) a distance of 2.32 Å, equal to  $3/2 \times 1.55$  Å, places the waters in the minimum of the free helix. As seen in Fig. 3, the water oxygen free energy profile in the absence of  $\text{Na}^+$  causes only a weak preference of water for specific sites along the helix axis. The presence of  $\text{Na}^+$  promotes the water-peptide hydrogen bonds of the two water molecules nearest to the ion in the helix. This in-phase sequence of the water-backbone hydrogen bonds ahead and behind the ion apparently gives rise to an “amplification” of the effect of water on the free energy barrier in for  $\text{Na}^+$ . The resulting contribution to the free energy barrier is 2.5 kcal/mol. The two nearest water molecules and their hydrogen bonds with the backbone carbonyl oxygens during the translocation of  $\text{Na}^+$  are indicated schematically in Fig. 7.

In the case of  $\text{K}^+$  ion the waters are displaced by  $2.71$  Å =  $7/4 \times 1.55$  Å. This places the waters out-of-phase with their natural periodicity in the helix and results in destructive interference of the water-backbone hydrogen bonds ahead and behind the ion. The water contribution to the potential of mean force of  $\text{K}^+$  is only 1.0 kcal/mol. More generally, coherence or interference of the ion size with the helix period of 1.55 Å is expected to lead to a significantly different water mean force contributions to the free energy profile of ions. An ion such as  $\text{Li}^+$  has an average water oxygen-ion distance of 2.0 Å. Due to its size, a water contribution smaller than for  $\text{Na}^+$  may be expected, everything else being equal, though the interaction energy is larger. Based on their Pauling radius  $\text{Rb}^+$  and  $\text{Cs}^+$  have an average water oxygen distance of 2.85 and 3.06 Å (1), respectively, suggesting that the water contribution is small.

The origin of the channel mean force contribution to the free energy profile of ions can also be understood in terms of the periodic helical structure. The sequence of peptide-peptide hydrogen bonds during translocation is illustrated schematically in Figs. 6 and 7, and in more details in Figs. 8 and 9. In the binding site, the  $\text{Na}^+$  ion is coordinated by four carbonyl oxygens (15, 20, 13, 18) located on the same side of the channel (see Fig. 6). The linear spacing of these four carbonyls along the channel axis is sufficiently large so that good oxygen- $\text{Na}^+$  contact is achieved with small dihedral distortions, and little stress in the helix. At the transition state, the  $\text{Na}^+$  ion is also making contact with four carbonyl oxygens (17, 15, 20, 18), but this time, located on opposite sides of the channel. This can be observed in Fig. 9. Larger helix distortions are necessary to achieve as good a coordination as in the binding site. This results in a slightly less stable situation for the whole system. The strong interactions with the ion in the system lead to the distortion of the hydrogen bonds of the helix backbone and to increased fluctuations at the transition state. For  $\text{K}^+$  the dihedral distortions are smaller due to the larger size of

the ion and they contribute negligibly to the activation energy. Finally, it should be noted that the “channel” contribution to the free energy barrier occurs where the linear density of carbonyl oxygen is the highest; i.e., exactly where the “water” free energy minimum was found.

## Applied external electric field

Information about the free energy profile of ions in the channel has been obtained experimentally from conductance measurements with a variety of ion concentration and applied transmembrane voltage. A way to introduce the effect of voltage to determine its effect on the potential of mean force is to use the constant electric field assumption (1, 16), i.e., it is assumed that the field does not vary over the dimension of the system. It is further assumed that the free energy profile is unchanged except for the superimposed external constant electric field  $E$ . If the transition state is located half-way between the successive binding sites, the rate constant becomes

$$k \rightarrow k_0 e^{-q\Delta V/k_B T}, \quad (23)$$

and

$$k' \rightarrow k'_0 e^{+q\Delta V/k_B T}, \quad (24)$$

where  $k$  ( $k_0$ ) are the forward rate constants in the presence (absence) of the field and  $k'$  ( $k'_0$ ) are the corresponding backward rate constants. The quantity  $\Delta V$  represents the change in electrostatic potential energy between the binding site and the transition state  $\Delta V = -qE\Delta x$ . In standard treatments the profile is extracted by adopting a kinetic scheme and adjusting the rates, modified with expressions like Eqs. 23 and 24 to account of the effect of voltage (5, 6). The underlying assumption is that the applied voltage acts only on the ion. However, to fit the experimental current-voltage curve, Eqs. 23 and 24 are incorrect, even to lowest order in the perturbation, because the free energy profile of an ion in presence of an applied voltage,  $\mathcal{W}(x; E)$ , should include the effect of the electric field on the charges associated with the channel. The perturbation technique allows us to study the effect of an applied external electric field on the entire system, including the helix. A correct treatment starts from a consideration of the Boltzmann configuration integral, Eq. 3,

$$e^{-\mathcal{W}(x; E)/k_B T} \propto \int dR e^{-U(R, x; E)/k_B T} \quad (25)$$

with the external field included as part of the total potential energy  $U(R, x; E)$

$$U(R, x; E) = U(R, x; 0) - qEx - \sum_i q_i Ex_i. \quad (26)$$

The external field is typically on the order of 100 mV over a distance of 26 Å. This is a relatively small perturbation on the scale of molecular interactions; e.g., a change of 100 mV applied to a unit charge is equivalent to 2.3 kcal/mol. A perturbation technique is thus an appropriate way to extract the deviation of the free energy profile relative to the unperturbed profile in presence of the applied field; i.e., we consider  $\delta\mathcal{W}(x; E) = \mathcal{W}(x; E) - \mathcal{W}(x; 0)$ , which we can write in the form

$$e^{-\delta\mathcal{W}(x; E)/k_B T} = \frac{\int dR e^{-U(R, x; E)/k_B T}}{\int dR e^{-U(R, x; 0)/k_B T}} = e^{qEx/k_B T} \langle e^{\sum_i q_i E_i / k_B T} \rangle_{U(R, x; 0)}. \quad (27)$$

A cumulant expansion (59) of the external field terms in Eq. 27 gives

$$\delta\mathcal{W}(x; E) \approx -qEx - \langle \mu(x) \rangle E + \frac{1}{2k_B T} \langle [\mu(x) - \langle \mu(x) \rangle]^2 \rangle E^2 + \dots \quad (28)$$

Truncating the expansion to first-order in the applied field, the contribution to  $\delta\mathcal{W}(x; E)$  from the remainder of the system is given by  $-\langle \mu(x) \rangle E$ , the average  $x$ -component dipole of the helix-water complex in the absence of the applied field  $E$  when the ion is located at the position  $x$ . The modified activation energy to first order in  $E$  is

$$\Delta\mathcal{W}^\ddagger = \Delta\mathcal{W}_0^\ddagger - (q\Delta x + \langle \Delta\mu \rangle)E, \quad (29)$$

where  $\Delta\mathcal{W}^\ddagger$  is the free energy of activation in the absence of the field  $E$  and  $\langle \Delta\mu \rangle$  is the change in the average dipole of the system (excluding the ion) when the ion goes from the bottom of the well to the transition state. The quantity  $\Delta x + \langle \Delta\mu \rangle/q$  is the “electric distance” between the bottom of the well and the top of the barrier (see Hille, page 257) (1). In standard treatments (as described above) the quantity  $\Delta x$  would be interpreted as a physical distance. With first-order perturbation theory, all averages are defined in the system in the absence of electric field; thus, it is not necessary to simulate the system in presence of an applied electric field, although a number of simulation studies have been done in the presence of an explicit applied potential to estimate the transport of ions in the gramicidin channel (i.e., the average drift of ions is monitored) (60, 61).

Convergence of the ensemble average of the dipole distortion induced by the ion is very slow and a series of direct averages of  $\mu(x)$  with the ion fixed at successive position is impractical. However, because we are only interested in the change in the dipole and not its absolute magnitude, the perturbation technique with Eq. 15 is an appropriate method for improving the statistical convergence. Using  $Q(x) = \mu(x)$  in Eq. 15, the

values of  $\langle \mu(x) \rangle$  are readily obtained from the simulations with the ion at various positions. The dipole profile induced by the  $\text{Na}^+$  ion is shown in Fig. 17. To get an idea of the magnitude of the distortion dipole  $\langle \Delta\mu \rangle$  it should be compared to the more standard correction to the activation energy  $q\Delta x$ . The distance  $\Delta x$  between the binding site and the transition state is equal to 0.75 Å. The calculation indicates that the average distortion dipole is on the order of  $0.4 \pm 0.2$  eÅ. This is a nonnegligible contribution to the activation free energy in presence of an applied field, resulting in an effective “electric distance” of 1.15 Å for the forward direction and 0.35 Å for the backward direction.

The dipole distortion arises from the libration of a few carbonyl groups, originally pointing in opposite directions. The libration of a single transpeptide amide plane (dipole = 0.85 eÅ) by 45° is sufficient to induce a distortion dipole of 0.4 eÅ. Calculated librations associated with the dihedral angles (Fig. 12) are in the range  $\pm 20$  degrees (55). More generally, the distortion dipole can increase or reduce the effective activation free energy barrier depending on the orientation of the distorted transpeptide amide planes with respect to the applied electric field. The combined effect of free energy barriers and distortion dipole effect may contribute to the mechanism of ion selectivity and nonohmic voltage response in biological channels.

For  $\text{K}^+$  the dihedral distortions are smaller and more delocalized than in the  $\text{Na}^+$  simulations so that the calculation of the distortion dipole induced by the  $\text{K}^+$  ion converged more slowly. Because the success of Eq. 15 in evaluating the distortion dipole depends on the degree to which the induced distortion is localized, no values are given for  $\text{K}^+$ . Based on the analysis of the free energy profile in the previous sections, it is clear that smaller ions introduce more local and larger distortions in the structure than larger ions. Consequently, the

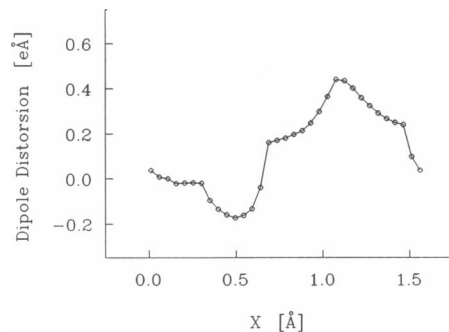


FIGURE 17 Helix dipole distortion induced by  $\text{Na}^+$  as it moves along the  $x$ -axis, the results are calculated with Eq. 15. The curve was corrected for a hysteresis of 0.2 eÅ by a linear correction.

dipole distortion contribution is expected to be more significant for the small ions than for the larger ions. A dipole distortion effect could be the source of the observed anomalous potential dependence of the small ions  $\text{Li}^+$  and  $\text{Na}^+$  in gramicidin A (6).

## Binding free energy difference

The global free energy difference of binding between two ions  $i$  and  $j$  can be calculated with the perturbation technique. For this purpose, the perturbation is in parameter space rather than in coordinate space. The calculation is an application of a free energy difference technique similar to Eqs. 4 and 15 with the van der Waals parameters  $A^{(8)}$  and  $B^{(6)}$  replacing the coordinate  $x$ . The difference in free energy, internal energy and entropy between two ions  $i$  and  $j$ ,  $\Delta\mathcal{A}_{ij}$ ,  $\Delta\mathcal{E}_{ij}$  and  $\Delta\mathcal{S}_{ij}$  are evaluated in the helix at constant  $x_0$ . For the free energy difference  $\mathcal{A}_{ij}$ , we have

$$e^{-\mathcal{A}_{ij}/k_B T} = \frac{\int dR e^{-U_i(R, x_0)/k_B T}}{\int dR e^{-U_j(R, x_0)/k_B T}}, \quad (30)$$

which is related to the difference in the absolute free energy profile,  $\mathcal{W}_i(x_0) - \mathcal{W}_j(x_0)$ , of two ions as calculated with Eq. 3.

Two ions of intermediate sizes between  $\text{Na}^+$  and  $\text{K}^+$  were found to be necessary to "mutate"  $\text{Na}^+$  into a  $\text{K}^+$  with satisfactory convergence. For the calculations the ions were constrained at a constant  $x_0$  chosen at the location of the free energy minimum of  $\text{Na}^+$ . The results are summarized in Table 6. The free energy difference  $\Delta\mathcal{A}$  is very sensitive to the choice of ion-carbonyl parameters used in the simulations and is examined in more details in the appendix for two  $\text{K}^+$  ion models. As expected, the free energy of the smaller ion is more negative due to a larger binding energy. This is partly balanced by a greater decrease in the entropy. This result contradicts the conclusion obtained from the study of Skerra and Brickmann (57), and of Brickmann and Fisher (56), based on nearly rigid gramicidinlike models. In a rigid channel model, the entropy is smaller for large ions due to the larger free volume available to the small ion. In a flexible model there is no such free volume around a small ion. The ion is able to distort the

helix locally and reorient the carbonyls because the ion-carbonyl interaction dominates the weaker peptides-peptides hydrogen bonds. This mechanism is not reproduced in rigid or nearly rigid models.

Using the experimental relative chemical potential of two ions  $i$  and  $j$  in bulk water ( $\Delta\mathcal{A}_{ij}^{\text{bulk}}$ ) (62, 63), it is possible to estimate their relative binding free energy in the helix. The ratio of the total binding constant must include the integration along the axis of the helix

$$\frac{K_i}{K_j} = e^{-[\Delta\mathcal{A}_{ij}^{\text{channel}} - \Delta\mathcal{A}_{ij}^{\text{bulk}}]/k_B T} \left[ \frac{\int_0^{\Delta L} e^{-[\mathcal{P}_i(x) - \mathcal{P}_i(x_0)]/k_B T} dx}{\int_0^{\Delta L} e^{-[\mathcal{P}_j(x) - \mathcal{P}_j(x_0)]/k_B T} dx} \right]. \quad (31)$$

In virtue of the periodicity of the integrands, the binding constant ratio can be expressed in terms of integrals over a single helical unit,  $\Delta L = 1.55 \text{ \AA}$ . The free energy profile of  $\text{Na}^+$  is considerably sharper and shows a strong oscillation that limit the translational configuration space whereas the profile is almost flat in the case of  $\text{K}^+$ . Evaluating the integral shows that

$$-k_B T \ln \left[ \frac{1}{\Delta L} \int_0^{\Delta L} e^{-[\mathcal{P}_{\text{Na}^+}(x) - \mathcal{P}_{\text{Na}^+}(x_0)]/k_B T} dx \right] = +1.0 \text{ kcal/mol.} \quad (32)$$

An unfavorable reduction in translational freedom decreases the binding free energy by  $\sim 1.0 \text{ kcal/mol}$  for  $\text{Na}^+$ . For  $\text{Na}^+$  and  $\text{K}^+$  the relative binding free energy is dominated by  $[\Delta\mathcal{A}_{ij}^{\text{channel}} - \Delta\mathcal{A}_{ij}^{\text{bulk}}]$ , with a small correction arising from the translational integral in Eq. 31. The binding constants determined from  $\text{Ti}^{+205}$  NMR, are  $31.6$  and  $58.4 \text{ M}^{-1}$  for  $\text{Na}^+$  and  $\text{K}^+$ , respectively (64). This corresponds to a difference in binding free energy of  $\sim k_B T$  between  $\text{Na}^+$  and  $\text{K}^+$ . Because the experimental the binding constants of  $\text{Na}^+$  and  $\text{K}^+$  differ only by a factor of two it is expected that  $\Delta\mathcal{A}_{ij}^{\text{channel}} \approx \Delta\mathcal{A}_{ij}^{\text{bulk}}$ . In bulk water the relative free energy of  $\text{Na}^+$  and  $\text{K}^+$ ,  $\Delta\mathcal{A}_{ij}^{\text{bulk}}$ , is  $20 \text{ kcal/mol}$  (62, 63). The difference in binding free energy is very sensitive to the parameterization of the ions. Using Eq. 31 these are  $\sim +14 \text{ kcal/mol}$  and  $\sim 0 \text{ kcal/mol}$  for model I and II of  $\text{K}^+$  ion, respectively (more details are given in the Appendix).

Contrary to the naive notion that a smaller ion must have more room than a larger ion in the channel, and therefore have a larger entropy, the entropy is more unfavorable for  $\text{Na}^+$  than for  $\text{K}^+$ . This is a direct consequence of the flexibility and the plasticity of the helix (51). The calculated entropy change,  $-T\Delta\mathcal{S}$  from  $\text{Na}^+$  to  $\text{K}^+$  is  $\sim 9.4 \text{ kcal/mol}$  in the helix and the experimental  $-T\Delta\mathcal{S}$  is  $\sim 2.6 \text{ kcal/mol}$  in water (62, 63); i.e., in both the channel and in bulk water the entropy of  $\text{Na}^+$  is less favorable than for  $\text{K}^+$ . The relative entropy of transfer from water to this position in the channel is thus  $\sim 6.8 \text{ kcal/mol}$ . The experimental estimate is  $\sim 1.0$

TABLE 6 Free energy perturbation (kcal/mol)\*

Transformations	$\Delta\mathcal{A}$	$\Delta\mathcal{E}$	$-T\Delta\mathcal{S}$
$\text{Na}^+$ to $\text{K}_I^+$	35.30	47.72	-8.42
$\text{Na}^+$ to $\text{K}_{II}^+$	20.37	33.44	-9.07

\*The average interaction energies are 203, 152, and 171 kcal/mol for  $\text{Na}^+$ ,  $\text{K}_I^+$  and  $\text{K}_{II}^+$ , respectively.

kcal/mol (64). It is known experimentally that the ion binding sites are located at the ends of the gramicidin channel (32), whereas we are looking at a site that is more representative of the interior of one of the monomers. It is possible that there are structural differences due to ends effect not taken into account in the periodic  $\beta$ -helix model. Also, the discrepancy may be caused in part by statistical errors due to insufficient sampling and to the inaccuracy of the potential functions. Nevertheless, the calculation indicates that the interior of the channel retains much of the solvation properties of a liquid in its interactions with the cations and that this is probably a more appropriate picture than a rigid helix. A similar conclusion was reached from experimental studies of ion binding in gramicidin (64). Due to the flexibility and plasticity of the  $\beta$ -helix the carbonyls respond to solvate the ion similarly to the waters surrounding the ion in the bulk.

## CONCLUDING DISCUSSION

This work demonstrates that statistical mechanical perturbation techniques can aid in understanding complex molecular systems like the gramicidin A channel. Although the absolute free energy of ions, such as  $\text{Na}^+$ , in a periodic  $\beta$ -helix model for the gramicidin channel is dominated by the strong ion-channel and ion-water interactions, the variations in the free energy profile are controlled by the weaker system–system interactions. The first coordination sphere of the ion (four carbonyls and two water molecules) contribute most of the solvation energy. However, the structure is so rigid that it is minimally distorted in going from the minimum to the transition state in the periodic helix. Thus, the energy leading to the transition state barrier is stored in the weaker interactions which adjust to the motion along the helix axis. As was first noted in a normal mode study (51), the flexibility of the  $\beta$ -helix is a fundamental property of the structure. Large correlated global motions have frequencies lower than  $75 \text{ cm}^{-1}$ , whereas local motions have higher frequencies. The carbonyl librations motions were located in the frequency band from 75 to  $175 \text{ cm}^{-1}$  and were localized in character. The transpeptide units (the rigid amide planes) were only weakly negatively correlated with one another, i.e., the anticorrelation was limited to the first hydrogen-bonded neighbors. The flexibility of the channel is an essential feature in its response to the presence of an ion. The distortion of the helix is significant but limited to a few carbonyls because the structure is too flexible to transmit a local distortion (such as a libration) to large distances. The plasticity of the structure (i.e., the property to deform without generating a large energy stress)

seems to be an essential factor in the transport of ions. The flexibility of the full dimer channel imbedded in a membrane may be influenced by the sidechains and the presence of the surrounding lipids. However, the peptide librational deformations, as already mentioned, do not involve global shape deformation of the channel. Thus, the distortions affecting the ion most directly are controlled by the local librations. Thus, the effect of the environment is likely to be small, analogous to the local high frequency fluctuations in the interior of proteins which are only slightly altered by the presence of solvent (20).

The mean force decomposition showed that the nearest two water molecules contribute  $\sim 2.5 \text{ kcal/mol}$  to a free energy barrier of  $4.5 \text{ kcal/mol}$ . The free energy profile of  $\text{Na}^+$  ion arises from both localized ion-water and ion-channel forces. However, the average ion-system “interaction energy” does not vary significantly from the bottom of the well to the transition state. In the binding sites the  $\text{Na}^+$  ion is surrounded by two water molecules and four carbonyls; two of these carbonyl contacts are maintained as the ion moves to the next binding site. This is seen to prevent any disruption of the solvation of the ion that would generate large free energy barrier opposing the translocation. Successive binding sites of four carbonyls are not truly independent of each other. Translocation of the  $\text{Na}^+$  ion occurs from one site to the next while retaining two carbonyls from the previous site. Structurally, the ion is not “hopping” from one site to the next leaving behind a nearly rigid cage of carbonyls. The plasticity of the helix prevents any disruption in the solvation of the ion and large variations in the ion-channel interaction energy. Even though the individual interaction of the  $\text{Na}^+$  with each of the carbonyls is quite large (on the order of  $38 \text{ kcal/mol}$ ), the flexibility of the helical structure is able to remove the very unfavorable steps of binding and unbinding to successive carbonyls that would generate a large ion-channel energy barrier opposing the translocation. The flexibility of the helix also plays a role in stabilizing the transition state by an increase in fluctuations (entropy) at the top of the barrier. This increase in entropy is mainly due to the local fluctuations at the transition state as illustrated in Fig. 5. The channel response to an applied external electric field was also estimated and shown to be significant in the case of  $\text{Na}^+$  ion. This observation casts some doubts on naive interpretation of the voltage dependent rate constants and their relation to the physical location of the free energy barrier in a channel.

On a methodological note, it is important to realize that the physical confinement of the system makes it very important to allow sufficient equilibration and sampling time. Although some recent work used curvilinear reac-

tion coordinate to describe the path of an ion in a periodic helix (65), our calculations show that the displacement of the ion along the helix axis relative to the center of mass of the helix is a convenient choice. To obtain converged results the ion position could be displaced only by a relatively small distance along the helix axis (0.1 Å). The choice of a periodic helix removed the complex effects of the end of the channel and made it possible to detect the magnitude of nonequilibrium hysteresis in the averaging. Even with great care, the computational method introduced a dissipative hysteresis of  $\sim +0.55$  kcal/mol Å.

Much remains to be done to reach a satisfactory understanding of ion transport through the gramicidin channel. Experimentally the rate of transport of  $\text{Na}^+$  and  $\text{K}^+$  differ only by a factor of two or so (4, 5, 7). Using arguments based on transition state theory, this corresponds to a difference on the order of 0.5 kcal/mol for the activation energy, much smaller than indicated by the present calculation (3.5 kcal/mol). Thus, further work will be necessary to investigate the similarity and the difference in the transport rate of  $\text{Na}^+$  and  $\text{K}^+$ . The empirical energy function, even though it was developed from high level *ab initio* calculations, is a possible source of error. However, the activation energy is mainly determined by the ion size and is not so sensitive to the absolute ion-carbonyl interaction energy. Thus, the present calculation suggests that the activation energy opposing the translocation of ions along the axis of the beta-helix is not the dominant factor in the relatively similar rate of transport observed experimentally. Other factors, (e.g., the barriers at the exit and entrance) may play the dominant role in the kinetics. The complex entrance and dehydration process, thought to be of paramount importance for a complete understanding of the permeability (7), has been left out of this preliminary study. Future work will focus on the analysis of the dynamics of ion translocation and the mobility of water,  $\text{Na}^+$  and  $\text{K}^+$  ions in the  $\beta$ -helix. The end effects in the finite gramicidin dimer will also be considered.

## APPENDIX A

### Parameter sensitivity

The sensitivity of the results to the choice of parameters is an important question. Although the  $\text{Na}^+$  and  $\text{K}^+$  carbonyl interaction were derived from high level *ab initio* calculations with a model peptide, the acetamide molecule, there is still a question as to the balance of the various interactions (ion-peptide, ion-water, water-water, peptide-peptide, and water-peptide). A way to determine the sensitivity of the results to the absolute interaction energy is to modify the empirical parameters to vary the well depth in such a way that the position of the minimum is unaffected. Because the geometries are more reliable than the energies, we have compared two  $\text{K}^+$  models which have the same minimum for the carbonyl-ion interaction of

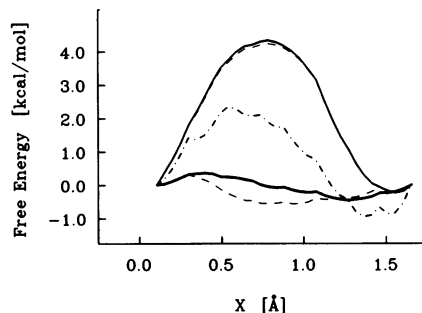


FIGURE 18 Free energy profiles perturbation calculated from Eq. 16. The solid line represents the initial  $\text{Na}^+$  and  $\text{K}^+$  profiles. The dashed line represents the altered ion-carbonyl interaction parameters  $K_{II}^{+}$ , described in the text. The dot-dashed line represent an intermediate ion smaller than  $\text{K}^+$  but larger than  $\text{Na}^+$ ; see also Fig. 2.

acetamide but have a different interaction energy (see Table 3). Both empirical models have an energy minimum at an ion-carbonyl distance of  $\sim 2.50$  Å in the acetamide energy surface. Using the simulation generated with the first  $\text{K}^+$  model, the parameters of a second  $\text{K}^+$  model were adjusted to yield better agreement with the experimental relative binding constant; i.e., the well depth of  $\text{K}^+$  model II was adjusted until the free energy difference with  $\text{K}^+$  model I is  $-15$  kcal/mol, giving a total free energy difference of  $+20$  kcal/mol relative to  $\text{Na}^+$  ion, similar to the experimental free energy difference between  $\text{K}^+$  and  $\text{Na}^+$  ion in bulk water (20 kcal/mol) (63). The results are summarized in Table 6 for the two  $\text{K}^+$  ion models. To obtain a total change of about 15 kcal/mol it is necessary to increase the interaction of  $\text{K}^+$  with the acetamide carbonyl oxygen by only 2.5 kcal/mol keeping the position of the energy minimum at 2.5 Å. The total interaction of  $\text{K}^+$  with one acetamide carbonyl was changed from 26.0 to 28.5 kcal/mol. This example shows how small changes in the parameters, within the accuracy of the empirical energy function, can affect the total free energy. Interestingly, the free energy profile of  $\text{K}^+$  ion model II calculated with Eq. 16, is not very affected by this modification, see Fig. 18. The free energy of activation for  $\text{K}^+$  remains close to 1.0 kcal/mol. The free energy profile of a perturbed  $\text{Na}^+$  ion, interacting with acetamide with an affinity decreased by 0.5 kcal/mol, is also shown in Fig. 18. The free energy profile of  $\text{Na}^+$  appears to be very insensitive to such perturbation. Comparison of the free energy profile of  $\text{Na}^+$  and  $\text{K}^+$  ions shows that the form of the potential is very sensitive to ion size. One may wonder how the transition from  $\text{Na}^+$  to  $\text{K}^+$  takes place. It is possible to estimate the free energy profile of a fictitious ion larger than  $\text{Na}^+$  but still smaller than  $\text{K}^+$  using the Eq. 16. The ion-acetamide interaction energy is shown in Fig. 2. The calculated free energy profile is shown in Fig. 18. The free energy of activation of the intermediate ion is  $\sim 2-3$  kcal/mol.

Most of the calculations were done at the Pittsburgh Supercomputing Center. Helpful discussions with David Busath, Hsiang Ai Yu, and Bruce Tidor are gratefully acknowledged. We thank Olaf. S. Andersen for a careful reading of the manuscript and John Roberts for help with the figures.

Supported in part by a grant from the National Science Foundation.

Received for publication 12 July 1990 and in final form 25 October 1990.

---

## REFERENCES

1. Hille, B. 1984. Ionic Channels of Excitable Membranes. Sinauer, Sunderland, MA.
2. Fisher, R., and T. Blumenthal. 1982. An interaction between gramicidin and the  $\sigma$  subunit of RNA polymerase. *Proc. Natl. Acad. Sci. USA.* 79:1045–1048.
3. Andersen, O. S. 1984. Gramicidin channels. *Annu. Rev. Physiol.* 46:531–548.
4. Hladky, S. B., and D. A. Haydon. 1972. Ion transfer across lipid membranes in the presence of gramicidin A. *Biochim. Biophys. Acta.* 274:294–312.
5. Hladky, S. B., and D. A. Haydon. 1984. Ion movements in gramicidin channels. *Curr. Top. Membr. Transp.* 21:327–372.
6. Eisenman, G., and R. Horn. 1983. Ionic selectivity revisited: the role of kinetic and equilibrium processes in ion permeation through channels. *J. Membr. Biol.* 76:197–225.
7. Finkelstein, A., and O. S. Andersen. 1981. The Gramicidin A Channel: a review of its permeability characteristics with special reference to the single-file aspect of transport. *J. Membr. Biol.* 59:155–171.
8. Chandler, D. 1978. Statistical mechanics of isomerization dynamics in liquids and the transition state approximation. *J. Chem. Phys.* 68:2959–2970.
9. Hynes, J. T. 1985. The theory of reactions in solutions. In *Theory of Chemical Reaction Dynamics*. M. Baer, editor. CRC Press, Boca Raton, FL. 171–235.
10. Cooper, K. E., P. Y. Gates, and R. S. Eisenberg. 1988. Surmounting barriers in ionic channels. *Q. Rev. Biophys.* 21:331–364.
11. Cooper, K. E., P. Y. Gates, and R. S. Eisenberg. 1988. Diffusion theory and discrete rate constant in ion permeation. *J. Membr. Biol.* 106:95–105.
12. Jordan, P. C. 1987. Microscopic approach to ion transport through transmembrane channels. The model system gramicidin. *J. Phys. Chem.* 91:6582–6591.
13. Chiu, S. W., and E. Jakobsson. 1989. Stochastic theory of singly occupied ion channels. II Effects of access resistance and potential gradient extending into the bath. *Biophys. J.* 55:147–157.
14. Glasstone, S., K. J. Laidler, and H. Eyring. 1941. Theory of Rate Processes. McGraw-Hill Inc., New York.
15. Läuger, P. 1982. Microscopic calculation of ion-transport rates in membrane channels. *Biophys. Chem.* 15:89–100.
16. Läuger, P. 1973. Ion transport through pores: a rate theory analysis. *Biochim. Biophys. Acta.* 311:423–441.
17. Levitt, D. G. 1986. Interpretation of biological channel flux data—reaction-rate theory versus continuum theory. *Annu. Rev. Biophys. Chem.* 15:29–57.
18. Roux, B., and M. Karplus. 1991. Ion transport in a gramicidin-like channel: dynamics and mobility. *J. Phys. Chem.* In press.
19. Hladky, S. B., and D. A. Haydon. 1974. Temperature-dependent properties of gramicidin A channels. *Biochim. Biophys. Acta.* 367:127–133.
20. Brooks III, C. L., M. Karplus, and B. M. Pettitt. 1988. Proteins. A theoretical perspective of dynamics, structure and thermodynamics. In *Advances In Chemical Physics*. Vol. 71. I. Prigogine and S. A. Rice, editors. John Wiley & Sons, Inc., New York.
21. Jordan, P. C. 1988. A molecular dynamics study of cesium ion motion in a gramicidin-like channel. In *Transport Through Membranes: Carriers, Channels and Pumps*. A. Pullman, B. Pullman, and J.G. Gortner, editors. Kluwer Academic Publishers, Norwell, MA. 237–251.
22. Åqvist, J., and A. Warshel. 1989. Energetics of ion permeation through membrane channels. *Biophys. J.* 56:171–182.
23. Pullman, A. 1987. Energy profiles in the gramicidin A channel. *Q. Rev. Biophys.* 20:173–200.
24. Kim, K. S., and E. Clementi. 1985. Energetics and hydration structure of a solvated gramicidin A channel for  $K^+$  and  $Na^+$  cations. *J. Am. Chem. Soc.* 107:5504–5513.
25. Mazet, J. L., O. S. Andersen, and R. E. Koeppe II. 1984. Single-channel studies on linear gramicidins with altered amino acid sequences. A comparison of phenylalanine, tryptophane and tyrosine substitutions at position 1 and 11. *Biophys. J.* 45:263–276.
26. Jorgensen, W. L., J. K. Bucker, S. E. Huston, and P. J. Rossky. 1987. Energy profiles for  $(CH_3)_3CCl$  ion pairs in aqueous solution. *J. Am. Chem. Soc.* 109:1891–1899.
27. Tobias, D. J., and C. L. Brooks III. 1987. Calculation of free energy surface using the methods of thermodynamic perturbation theory. *Chem. Phys. Lett.* 142:472–476.
28. Tobias, D. J., and C. L. Brooks III. 1990. The thermodynamics of solvophobic effects: a molecular-dynamics study of *n*-butane in carbene tetrachloride and water. *J. Chem. Phys.* 92:2582–2592.
29. Mazor, M., and M. B. Pettitt. 1990. Convergence of the chemical potential in aqueous simulations. *Molecular Simulations*. In press.
30. Arseniev, A. S., V. F. Bystryov, T. V. Ivanov, and Y. A. Ovchinnikov. 1985.  $^1H$ -NMR study of gramicidin-A transmembrane ion channel. Head-to-head right-handed, single stranded helices. *FEBS (Fed. Eur. Biochem. Soc.) Lett.* 186:168–174.
31. Urry, D. W. 1971. The Gramicidin A transmembrane channel: a proposed  $\pi_{LD}$  helix. *Proc. Natl. Acad. Sci. USA.* 68:672–676.
32. Urry, D. W., K. U. Prasad, and T. L. Trapane. 1982. Location of monovalent cation binding sites in the gramicidin channel. *Proc. Natl. Acad. Sci. USA.* 79:390–394.
33. Cornell, B. A., F. Separovic, A. J. Baldassi, and R. Smith. 1988. Conformation and orientation of gramicidin A in oriented phospholipid bilayers measured by solid state carbon-13 NMR. *Biophys. J.* 53:67–76.
34. LoGrasso, P. V., L. K. Nicholson, and T. A. Cross. 1989. N—H bond length determinations and implications for the gramicidin channel conformation and dynamics from  $^{15}N$ — $^1H$  dipolar interactions. *J. Am. Chem. Soc.* 111:1910–1912.
35. Smith, R., D. E. Thomas, F. Separovic, A. R. Atkins, and B. A. Cornell. 1989. Determination of the structure of a membrane-incorporated ion channel. *Biophys. J.* 56:307–314.
36. Nicholson, L. K., and T. A. Cross. 1989. The gramicidin cation channel: an experimental determination of the right-handed helix sense and verification of  $\beta$ -type hydrogen bonding. *Biochemistry.* 28:9379–9385.
37. Bystryov, V. F., and A. S. Arseniev. 1988. Diversity of the gramicidin A spatial structure: two-dimensional  $^1H$ -NMR study in solution. *Tetrahedron.* 44:925–940.
38. Urry, D. W., and C. M. Venkatachalam. 1983. Theoretical conformation analysis of the gramicidin A transmembrane channel. I. Helix sense and the energetics of head-to-head dimerization. *J. Comput. Chem.* 4:461–469.
39. Brooks, B. R., R. E. Bruccoleri, B. D. Olafson, D. J. States, S. Swaminathan, and M. Karplus. 1983. CHARMM: a program for

- macromolecular energy minimization and dynamics calculations. *J. Comput. Chem.* 4:187.
40. Chiu, S. W., S. Subramaniam, E. Jakobsson, and J. A. McCammon. 1989. Water and polypeptide conformation in the gramicidin channel. *Biophys. J.* 56:253–261.
41. Jorgensen, W. L., R. W. Impey, J. Chandrasekhar, J. D. Madura, and M. L. Klein. 1983. Comparison of simple potential functions for simulating liquid water. *J. Chem. Phys.* 79:926–935.
42. Lifson, S., A. T. Hagler, and P. Dauber. 1979. Consistent force field studies of inter-molecular forces in hydrogen-bonded crystals. *J. Am. Chem. Soc.* 101:5111–5141.
43. Belle, D. V., I. Couplet, M. Prevost, and S. J. Wodak. 1987. Calculations of electrostatic properties in proteins. *J. Mol. Biol.* 198:721–735.
44. Goodfellow, J. M., J. L. Finney, and P. Barnes. 1982. Monte Carlo computer simulation of water-amino acid interactions. *Proc. R. Soc. Lond. B. Biol. Sci.* 214:213–228.
45. Lybrand, T. P., and P. A. Kollman. 1985. Water-water and water-ion potential functions including terms for many body effects. *J. Phys. Chem.* 83:2923–2933.
46. Zwanzig, R. W. 1954. High temperature equation of state by a perturbation method. *J. Chem. Phys.* 22:1420–1426.
47. McQuarrie, D. A. 1976. Statistical Mechanics. Harper and Row, New York.
48. Gao, J., K. Kuczera, B. Tidor, and M. Karplus. 1989. Hidden thermodynamics of mutant proteins: a molecular dynamics study. *Science (Wash. DC)*. 244:1069–1072.
49. Yu, H. A., and M. Karplus. 1988. A thermodynamic analysis of solvation. *J. Chem. Phys.* 89:2366.
50. Gunsteren, W. F., and H. J. C. Berendsen. 1977. Algorithms for macromolecular dynamics and constraint dynamics. *Mol. Physiol.* 34:1311–1327.
51. Roux, B., and M. Karplus. 1988. The normal modes of the gramicidin A dimer channel. *Biophys. J.* 53:297–309.
52. Mackay, D. H., P. H. Berens, and K. R. Wilson. 1983. Structure and dynamics of ion transport through gramicidin A. *Biophys. J.* 46:229–248.
53. Urry, D. W., C. M. Venkatachalam, K. U. Prasad, R. J. Bradley, G. Parenti-Castelli, and G. Lenaz. 1981. Conduction process of the gramicidin channel. *Int. J. Quant. Chem. Quant. Biol. Symp.* 8:385–399.
54. Fleischman, S. H., and C. L. Brooks III. 1987. Thermodynamics of aqueous solvation. *J. Chem. Phys.* 87:3029–3037.
55. Yu, H. A., and M. Karplus. 1990. An integral equation study of the solvent-induced reaction barrier in the nucleophilic addition of hydroxide to formaldehyde. *J. Am. Chem. Soc.* 112:5706–5716.
56. Brickmann, J., and W. Fisher. 1983. Entropy effects on the ion diffusion rate in transmembrane protein channels. *Biophys. Chem.* 17:245–256.
57. Skerra, A., and J. Brickmann. 1987. Structure and dynamics of one-dimensional ionic solutions in biological transmembrane channels. *Biophys. J.* 51:969–976.
58. Lee, W. K., and P. C. Jordan. 1984. Molecular dynamics simulation of cation motion in water-filled gramicidin-like pore. *Biophys. J.* 46:805–819.
59. Balescu, R. 1975. Equilibrium and Non-Equilibrium Statistical Mechanics. John Wiley and Sons, Inc., New York.
60. Skerra, A., and J. Brickmann. 1987. Simulation of voltage-driven hydrated cation transport through narrow transmembrane channels. *Biophys. J.* 51:977–983.
61. Kim, K. S. 1985. Microscopic effect of an applied voltage on the solvated gramicidin A transmembrane channel in the presence of  $\text{Na}^+$  and  $\text{K}^+$  cations. *J. Comp. Chem.* 6:256–263.
62. Marcus, Y. 1986. The hydration entropies of ions and their effects on the structure of water. *J. Chem. Soc. Faraday Trans. I.* 82:233–242.
63. Marcus, Y. 1987. The thermodynamics of solvation of ions. Part 2. *J. Chem. Soc. Faraday Trans. I.* 83:339–349.
64. Hinton, J. F., J. Q. Fernandez, D. C. Shungu, W. L. Whaley, R. E. Koeppe II, and F. S. Millett. 1988. TI-205 nuclear magnetic resonance determination of the thermodynamic parameters for the binding of monovalent cations to gramicidin A and C. *Biophys. J.* 54:527–533.
65. Schröder, H. 1985. Rate theory analysis of ion-selectivity in membrane channels with elastically bound ligands. *Eur. Biophys. J.* 12:129–142.
66. Hehre, W. J., R. Ditchfield, and J. A. Pople. 1972. Self-consistent molecular orbital methods. XII. Further extension of gaussian-type basis sets for use in molecular orbital studies of organic molecules. *J. Chem. Phys.* 56:2257.